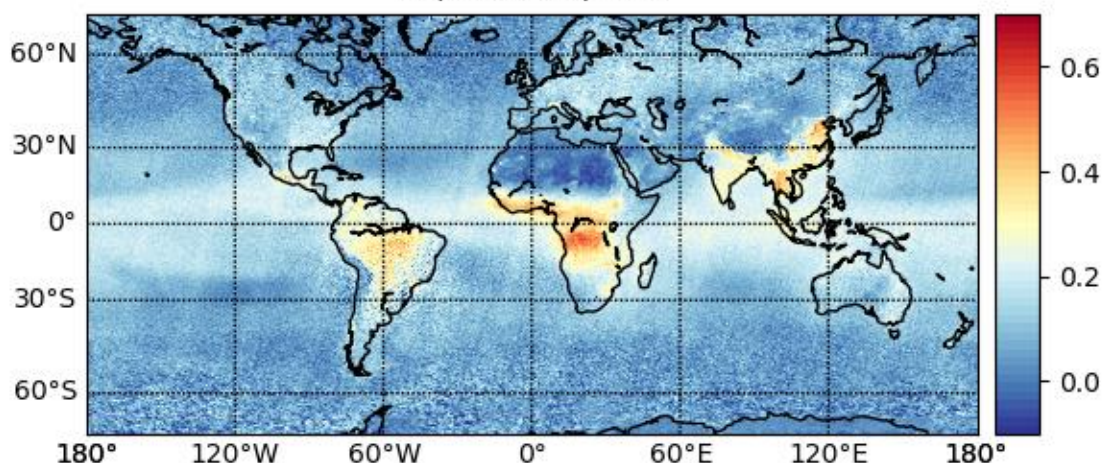


AC SAF VALIDATION REPORT

Validated products:

Name	Acronym
CHOCHO Data Records from GOME-2 on Metop-A and Metop-B	O3M-120

GOME2A CHOCHO VCD (Pmolec.cm-2)
01/2007-12/2017



Authors:

Name	Institute
Michel Van Roozendael	Royal Belgian Institute for Space Aeronomy
Christophe Lerot	Royal Belgian Institute for Space Aeronomy
François Hendrick	Royal Belgian Institute for Space Aeronomy
Gaia Pinardi	Royal Belgian Institute for Space Aeronomy
Pieter Valks	German Aerospace Center

Reporting period: GOME-2A: January 2007 – December 2017
GOME-2B: January 2013 – June 2020

Input data versions: GOME-2 Level 1B version 6.3

Data processor versions: G2_L2_GLY version 1.0

reference SAF/AC/IASB/VR/CHOCHO/TN-IASB-GOME2AB-ACSAF-CHOCHO-2020
document type AC SAF Validation Report
issue 1
revision 2
date of issue 08 February 2021
products O3M-120
product version level-0-to-1: v6.3 ; level-1-to-2: v1.0
distribution

Function	Organisation
AC SAF	EUMETSAT, BIRA-IASB, DLR, DMI, DWD, FMI, HNMS/AUTH, KNMI, LATMOS, RMI
UPAS Team	DLR-IMF, DLR-DFD
Ground-based data providers	BIRA-IASB, ChibaU

external contributors

contributing ground-based correlative measurements

Acronym	Organisation	Peoples
BIRA-IASB	Royal Belgian Institute for Space Aeronomy, Belgium	M. Van Roozendael, F..Hendrick, C. Fayt, C. Hermans
ChibaU	Center for Environmental Remote Sensing, Chiba University, Chiba, Japan	Hitoshi Irie and Chiba University team

document change record

Issue	Rev.	Date	Section	Description of Change
1	0	14.10.2020	all	Creation of this document
1	1	14.12.2020	all	Final document
1	2	08.02.2021	all	Document modified according to RIDs raised during the review

AC SAF product ID numbers

AC SAF internal identifier	Description
CHOCHO Data Record, GOME-2 Metop-A and Metop-B	O3M-120

Validation report of GOME-2 CHOCHO total column data records for Metop-A and Metop-B

CONTENTS

ACRONYMS AND ABBREVIATIONS.....	4
INTRODUCTION TO EUMETSAT SATELLITE APPLICATION FACILITY ON ATMOSPHERIC COMPOSITION MONITORING (AC SAF).....	5
DATA DISCLAIMER FOR THE METOP-A AND METOP-B GOME-2 TOTAL CHOCHO DATA RECORDS.....	7
A. INTRODUCTION.....	9
A.1. Scope of this document.....	9
A.2. Preliminary remarks	9
A.3. Plan of this document	9
B. GOME-2 GLYOXAL RETRIEVAL APPROACH.....	10
B.1 DOAS slant column fitting.....	10
B.2 Reference radiance spectrum and reference sector correction.....	10
B.3 AMF and VCD determination	11
B.4 Impact of the noise and need for averaging data	12
C. INTER-SATELLITE COMPARISONS.....	14
D. COMPARISONS WITH GROUND-BASED MEASUREMENTS	25
D1. Ground-based MAX-DOAS data sets description	25
D2. Comparison results.....	26
E. CONCLUSIONS	31
F. REFERENCES	33
G.1. Applicable documents	33
G.2. Reference.....	33
G.2.1 Peer-reviewed articles.....	33

ACRONYMS AND ABBREVIATIONS

AC SAF	Atmospheric Composition Monitoring Satellite Application Facility
AMF	Air Mass Factor, or optical enhancement factor
BIRA-IASB	Belgian Institute for Space Aeronomy
CHOCHO	Glyoxal
DLR	German Aerospace Centre
DOAS	Differential Optical Absorption Spectroscopy
ESA	European Space Agency
EUMETSAT	European Organisation for the Exploitation of Meteorological Satellites
FRM4DOAS	Fiducial Reference Measurements for Ground-Based DOAS Air-Quality Observations
GDP	GOME Data Processor
GEOMS	Generic Earth Observation Metadata Standard
GOME	Global Ozone Monitoring Experiment
HCHO	Formaldehyde
IMF	Remote Sensing Technology Institute
LOS	Line Of Sight
MAXDOAS	Multi Axis Differential Optical Absorption Spectroscopy
MPC	Mission Performance Center
NDACC	Network for the Detection of Atmospheric Composition Change
O ₃	Ozone
OCRA	Optical Cloud Recognition Algorithm
OMI	Ozone Monitoring Instrument
QA4ECV	Quality Assurance for Essential Climate Variables
ROCINN	Retrieval of Cloud Information using Neural Networks
RRS	Rotational Raman Scattering
SCD	Slant Column Density
SNR	Signal to Noise Ratio
SZA	Solar Zenith Angle
TROPOMI	TROPOspheric Monitoring Instrument
UPAS	Universal Processor for UV/VIS Atmospheric Spectrometers
UVVIS	Ultraviolet-visible spectrometry
VCD	Vertical Column Density
WMO	World Meteorological Organization

INTRODUCTION TO EUMETSAT SATELLITE APPLICATION FACILITY ON ATMOSPHERIC COMPOSITION MONITORING (AC SAF)

Background

The monitoring of atmospheric chemistry is essential due to several human-induced changes in the atmosphere, like global warming, loss of stratospheric ozone, increasing UV radiation, and pollution. Furthermore, it is used to react to threats caused by natural hazards as well as to follow the effects of international protocols.

Therefore, monitoring the chemical composition and radiation of the atmosphere is a very important duty for EUMETSAT and the target is to provide information for policy makers, scientists and general public.

Objectives

The main objectives of the AC SAF is to process, archive, validate and disseminate atmospheric composition products (O₃, NO₂, SO₂, BrO, HCHO, CHOCHO, H₂O, OClO, CO, NH₃), aerosol products and surface ultraviolet radiation products utilising the satellites of EUMETSAT. The majority of the AC SAF products are based on data from the GOME-2 and IASI instruments onboard Metop satellites.

Another important task besides the near real-time (NRT) and offline data dissemination is the provision of long-term, high-quality atmospheric composition products resulting from reprocessing activities.

Product categories, timeliness and dissemination

NRT products are available in less than three hours after measurement. These products are disseminated via EUMETCast, WMO GTS or internet.

- Near real-time trace gas columns (total and tropospheric O₃ and NO₂, total SO₂, total HCHO, CO) and high-resolution ozone profiles
- Near real-time absorbing aerosol indexes from main science channels and polarization measurement detectors
- Near real-time UV indexes, clear-sky and cloud-corrected

Offline products are available within two weeks after measurement and disseminated via dedicated web services at EUMETSAT and AC SAF.

- Offline trace gas columns (total and tropospheric O₃ and NO₂, total SO₂, total BrO, total HCHO, total H₂O) and high-resolution ozone profiles
- Offline absorbing aerosol indexes from main science channels and polarization measurement detectors
- Offline surface UV, daily doses and daily maximum values with several weighting functions

Data records are available after reprocessing activities from the EUMETSAT Data Centre and/or the AC SAF archives.

- Data records generated in reprocessing
- Lambertian-equivalent reflectivity
- Total OClO

Users can access the AC SAF offline products and data records (free of charge) by registering at the AC SAF web site.

More information about the AC SAF project, products and services: <https://acsaf.org/>

AC SAF Helpdesk: helpdesk@acsaf.org

Twitter: https://twitter.com/Atmospheric_SAF

DATA DISCLAIMER FOR THE METOP-A AND METOP-B GOME-2 TOTAL CHOCHO DATA RECORDS

In the framework of EUMETSAT's Atmospheric Composition Monitoring Satellite Application Facility (AC SAF), GOME-2 glyoxal (CHOCHO) total column data product are generated at DLR from Metop-A and Metop-B GOME-2 measurements using the level-0-to-1: v6.3 processor and the level-1-to-2 G2_L2_GLY DOAS retrieval processor (see TN-DLR-ATBD and TN-DLR-PUM).

This report presents the verification of GOME-2 CHOCHO column from Metop-A (2007-2017) and Metop-B (2012-2017) obtained with the G2_L2_GLY processor. CHOCHO column data were investigated through:

- 1) verification of their consistency with scientific retrievals applied to the Aura OMI and Sentinel-5p TROPOMI instruments;
- 2) evaluation against ground-based observations from a selection of 5 MAX-DOAS instruments.

The main results from the validation are summarized hereafter:

1. Glyoxal satellite products are prone-to-noise due to the low optical depth of the measured absorption signal (typically less than 0.001). Averaging a sufficient number of individual observations is necessary to lower the random noise, extract meaningful glyoxal signals and eventually identify possible systematic differences between satellite or ground-based instruments. This is obtained at the cost of time and/or space resolution. Typically, combining data over one full month is a good trade-off for reliable comparisons.
2. GOME-2A and GOME-2B glyoxal VCDs are in general good agreement with both OMI and TROPOMI sensors. All instruments observe similar seasonalities, and reported VCDs are in the same range of magnitude. The two GOME-2 data sets show an excellent level of mutual agreement.
3. In some regions, a systematic difference is found between mid-morning GOME-2 and early afternoon OMI and TROPOMI data, which is likely to be due to actual diurnal variation effects.
4. Long-term time-series of GOME-2A and GOME-2B show an excellent level of stability in comparison to reference data.
5. These conclusions are valid in all regions investigated in the report, including the more challenging mid-latitudes where the combination of the lower glyoxal concentrations and lower sun elevation make the retrievals more difficult.
6. Based on an analysis of the median differences with OMI and TROPOMI data, we conclude that all sensors agree within 1.5×10^{14} molec.cm⁻², corresponding to about 30% of median values. Accordingly, the GOME-2 glyoxal products meet the optimum accuracy requirements of 30 % for polluted conditions.
7. The mean relative bias between GOME-2A and MAX-DOAS glyoxal VCDs at five stations is between -33.2% and +5.5%, which is close to the optimum accuracy requirement of 30%.
8. The mean bias between GOME-2B and MAX-DOAS data is comprised between -40.0% and +31.1%, i.e. within the target accuracy requirements of 50%.
9. MAX-DOAS comparison results suggest that GOME-2B data are slightly noisier than GOME-2A ones. They also indicate that satellite data show a tendency to underestimate

MAX-DOAS values. This underestimation can be partly mitigated by applying satellite averaging kernels to the ground-based MAX-DOAS profiles.

A. INTRODUCTION

A.1. Scope of this document

The present document reports on the verification and geophysical validation of GOME-2/Metop-A CHOCHO column data acquired over the 2007-2017 period and GOME-2/Metop-B data acquired over the 2012-2017 period. The data were produced by the G2_L2_GLY v1.0 processor operated at the DLR Remote Sensing Technology Institute (DLR-IMF, Oberpfaffenhofen, Germany) in the framework of the EUMETSAT AC SAF. This report addresses the verification of the Metop-A and Metop-B CHOCHO data records using mutual consistency checks, comparison with independent satellite retrievals from the Aura OMI and Sentinel-5p TROPOMI sensors and comparison with ground-based MAX-DOAS reference data sets. The goal is to investigate the overall consistency of the GOME-2 CHOCHO data records and to assess whether the product fulfils the user requirements in term of accuracy (threshold 100%, target 50% and optimal 30% for polluted conditions), as stated in the ACSAF Product Requirement Document (version 1.7, 01/09/2020).

A.2. Preliminary remarks

To report on the status of the verification of the Metop-A and Metop-B GOME-2 glyoxal columns, comparisons are performed based on (1) reference glyoxal data products generated at BIRA-IASB from OMI and TROPOMI sensors, and (2) ground-based MAX-DOAS correlative data performed at BIRA-IASB stations as well as additional stations operated by the Chiba University in Asia. The consistency of the different glyoxal products is explored by performing comparisons with these available correlative data sets. It should be noted that this part relies on scientific data products made available on purpose for this exercise, and not necessarily fully assessed and validated. In particular MAX-DOAS data sets are based on non-harmonised scientific retrievals independently performed at BIRA-IASB and at Chiba University, using different retrieval approaches. This particularity must be taken into consideration when interpreting the validation results.

A.3. Plan of this document

After presentation of the AC SAF introduction and the GOME-2 Data Disclaimer for CHOCHO column products, this document is divided into the following sections:

- A.** Introduction
- B.** GOME-2 glyoxal retrieval approach
- C.** Inter-satellite comparisons
- D.** Comparisons with ground-based measurements
- E.** Conclusion
- G.** References

B. GOME-2 GLYOXAL RETRIEVAL APPROACH

B.1 DOAS slant column fitting

The DOAS algorithm for glyoxal (CHOCHO) is based on the DOAS algorithm for ozone, as described in [TN-DLR-ATBD]. The CHOCHO columns are retrieved in the wavelength range 435-460 nm, and the settings include a cross-section for the liquid water absorption signature in addition to cross-sections of other atmospheric absorbers. The details of the DOAS algorithm used for CHOCHO retrieval are listed in Table B1.

Table B1: DOAS settings used to retrieve glyoxal slant columns.

Fitting interval	435-460 nm
Absorption cross-sections	
Glyoxal	Volkamer et al. (2005)
Ozone	Serdyuchenko et al. (2014), 223K
H ₂ O (vapor)	Rothman et al. (2013), 293K
NO ₂	Vandaele et al. (1998), 220 and 294K
O ₄ (O ₂ -O ₂)	Thalman and Volkamer (2013), 293K
H ₂ O (liquid)	Mason et al. (2016) (SCD constrained by value retrieved in 405-490 nm interval)
Ring effect	Pseudo-absorber (Chance and Spurr, 1997)
Resolution change	Pseudo-absorber (Beirle et al., 2017)
Polarisation correction	Eta, Zeta from GOME-2 calibration key data (EUMETSAT, 2011)
Polynomial	3 rd order
Intensity offset correction	First order offset (additional cross-section taken as the inverse of the reference spectrum)
Earthshine wavelength Doppler-shift	Shift and stretch
Reference spectrum (E0)	Daily average of radiances, selected in equatorial Pacific ([-20° 20°], Long: [150°E-110°W]); CF<0.2)

B.2 Reference radiance spectrum and reference sector correction

In the DOAS retrievals, the daily irradiance spectra measured by GOME-2 are usually used. However, their usage introduces yearly reproducible time-dependent offsets in the retrieved CHOCHO slant columns (Lerot et al., 2010). To solve the problem related to the irradiance spectra, the daily averaged radiances selected in the region (Latitude: 45° S- 45° N; Longitude: 170° E- 130° W; SZA: 30-50; cloud fraction less than 0.2) are used as the reference. In addition, a daily normalization procedure based on measurements in remote Pacific Ocean is applied, as commonly used for minor trace gas retrievals (Richter et al., 2002).

A differential correction value $N_{s,0}$ to be applied to all retrieved slant columns is determined as the mean difference between all slant columns $N_{s,ref}$ of pixels falling into the reference sector and the corresponding calculated reference slant column based on the reference value $N_{v,0,ref}$ of 1×10^{14} molec.cm⁻²:

$$N_{s,0} = \overline{(N_{s,ref} - N_{v,0,ref} \times M_{ref})}$$

where M_{ref} is the AMF of pixels belonging to the reference sector. The normalization value of 1×10^{14} molec.cm⁻² is roughly consistent with the non-normalization vertical columns averaged in the reference sector (Lerot et al., 2010). The differential correction values are then added to all retrieved slant columns before their conversion into the vertical columns. The reference sector is defined by pixels with longitudes ranging between 180°W and 135°W. The normalization procedure is in practice applied in two steps. The first step of the procedure applies a VZA-dependent normalization based on retrievals in the equatorial part of the reference sector [$\pm 15^\circ$ latitude]. Then a linear latitudinal-dependent normalization is applied. This second part is based on the fit of a linear polynomial through mean differential correction values computed in 10° latitude bins between 70°N and 70°S. Note that only pixels within the reference sector with cloud fraction less than 0.2 and low liquid water SCDs ($SCD_{LW} < 100$) are considered.

B.3 AMF and VCD determination

The AMF depends strongly on the vertical profile shape of CHOCHO in the troposphere, the surface albedo and the presence of clouds. Since CHOCHO is an optically thin absorber in this wavelength region, the air mass factor is calculated by decoupling the radiative transfer calculations from the trace gas profile shape:

$$M = \frac{\sum_l m_l(\mathbf{b})x_l}{\sum_l x_l}$$

where m_l is the air mass factors for the individual layer l (independent of the CHOCHO profile), \mathbf{b} represents a set of forward model parameters including the GOME-2 viewing geometry, surface albedo, clouds and aerosols, and x_l the partial CHOCHO column in layer l . The altitude-dependent air mass factors m_l are calculated with the LIDORT radiative transfer model for 448 nm.

Two different approaches are used depending on the surface condition. Over land, the a priori CHOCHO profiles are provided by the IMAGES version 2 chemical transport model (Stavrakou et al., 2009). These profiles are calculated on a monthly basis at a horizontal resolution of 2.0° latitude by 2.5° longitude, with 40 vertical layers extending from the surface up to ~ 44 hPa. For the air mass factor computation, CHOCHO profiles are extracted from a climatology built using 10 years of model runs. Over the ocean, a measured CHOCHO profile over Pacific during the TORERO campaign (Volkamer et al., 2015) is used. The surface albedo is derived from version 3 of the GOME-2 directionally dependent Lambertian-equivalent reflectivity (DLER) -database at 452 nm, as described in Tilstra et al. (2017).

The computation of the CHOCHO vertical column density V then proceeds via:

$$V = \frac{S + \Delta S}{M}$$

where S is the retrieved slant column and ΔS is the normalization term computed from the background correction procedure in the Pacific reference sector, as described above. For many measurements over cloudy scenes, the cloud-top is well above the CHOCHO abundance in the boundary layer, and when the clouds are optical thick, the enhanced tropospheric CHOCHO concentrations cannot be detected by GOME-2. Therefore, only the CHOCHO vertical columns retrieved for observations with clear sky (Cloud fraction $< 20\%$) are provided in the GOME-2 L2 product.

B.4 Impact of the noise and need for averaging data

Because of the very low optical depth of the measured absorption features, glyoxal retrievals are significantly impacted by the shot-noise of the radiance measurements. As a consequence, individual glyoxal measurements at a given location and time present a significant scatter, which is generally much larger than the actual physical glyoxal signal.

Fortunately, this type of error is random and can be reduced by averaging a series of observations. Depending on the needs, space or time resolution can be favored at the cost of the other. The distribution of observations scattered because of random processes follows a Gaussian law and therefore, the random error is reduced by a factor $1/\sqrt{N}$ when averaging N observations.

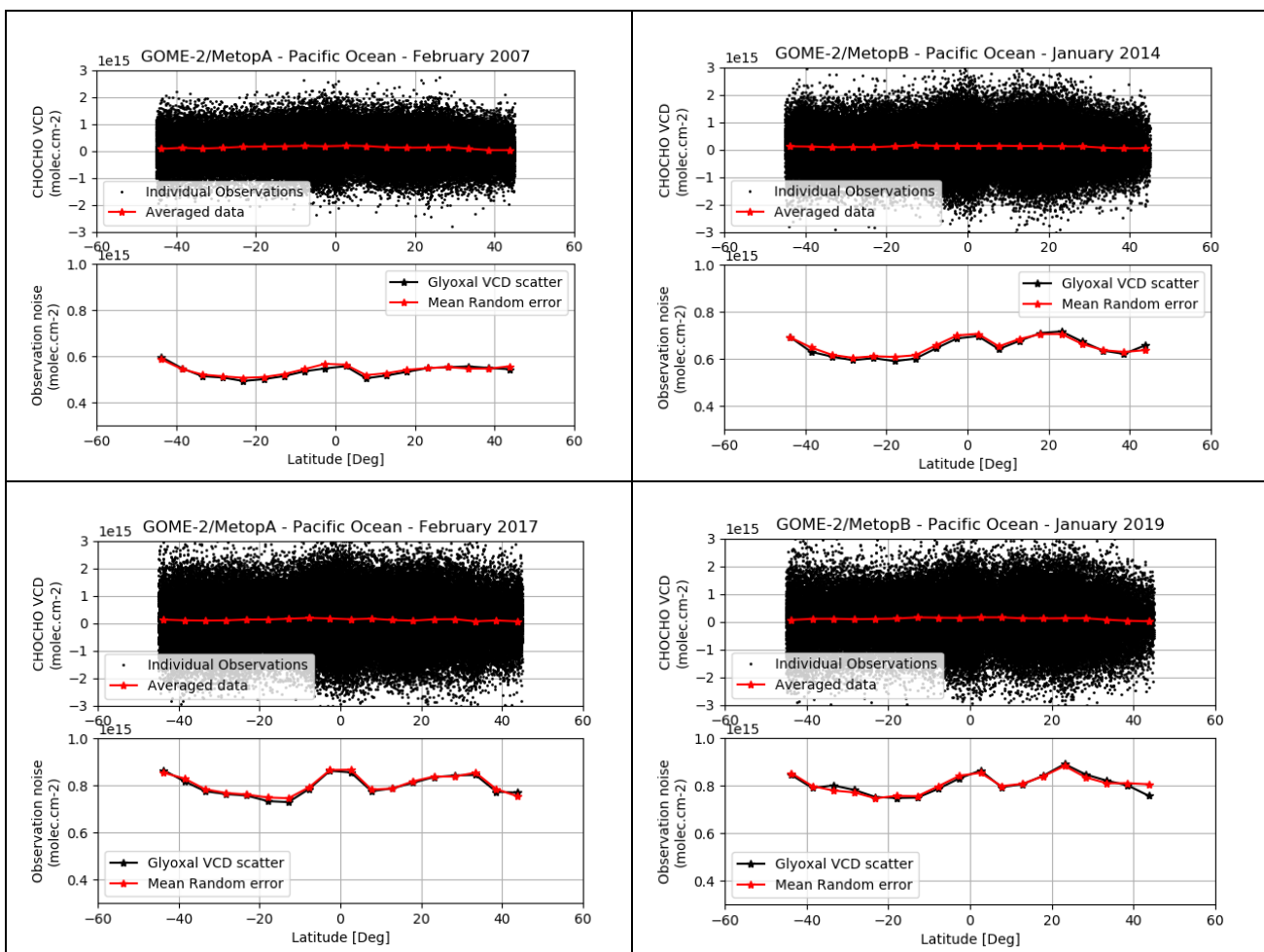


Figure B1: Illustration of the large scatter in glyoxal retrievals from GOME-2A (left figures) and GOME-2B (right figures) in a longitude band over the Pacific Ocean. Each figure show in the upper panel all individual glyoxal vertical column retrievals during a period of one month as well as averaged data in 5° latitude bins. The lower panels show the standard deviation of individual data in those 5° latitude bins and the mean estimated random errors. The upper row corresponds to one month at the early stage of the missions, while the lower row corresponds to a month after a few years of operations.

Figure B1 illustrates the large scatter of the GOME-2A/B glyoxal retrievals over a remote region in the Pacific Ocean where the real glyoxal signal is expected to be small. Individual observations (black dots) can be high- or low-biased because of the noise in the radiance measurements. When a large number of individual measurements are combined (here in 5° -latitude bins), the random error is reduced by the square root of the number of points, revealing a more physical quantity (very small in this example). The figure also shows that the random error estimates as provided in

the GOME-2A/B products agree well with the observed standard deviation of the individual measurements. Because of instrumental degradation, the random error generally increases over time. This is also illustrated in Figure B.1 where the observation noise is larger after a few years of operation (lower panels) than at the early phase of the operations (upper panels).

Figure B2 illustrates even more clearly the need of averaging data to extract meaningful glyoxal signal. This figure shows time series of GOME-2A and GOME-2B glyoxal measurements over South-Central Africa where emissions of glyoxal and of its precursors are very important. The figure shows in black daily mean glyoxal vertical columns. A large number of observations (typically > 100) have been combined every day allowing to distinguish the real glyoxal columns and their variability. They typically range between 2 and 6×10^{14} molec.cm⁻² in this region. Note that the noise can be further reduced by combining several days of data together (see e.g. 30-day running averages in red). The magenta lines represent the time series of the mean signal plus/minus the standard deviation of the points considered in the daily mean. These clearly indicate that averaging is essential to detect a meaningful signal.

In the next sections of this report, glyoxal data, originating either from space or from ground-based instruments, are averaged in space and time before being intercompared. This approach allows a comparison of the noise-free column fields and the identification of possible systematic differences.

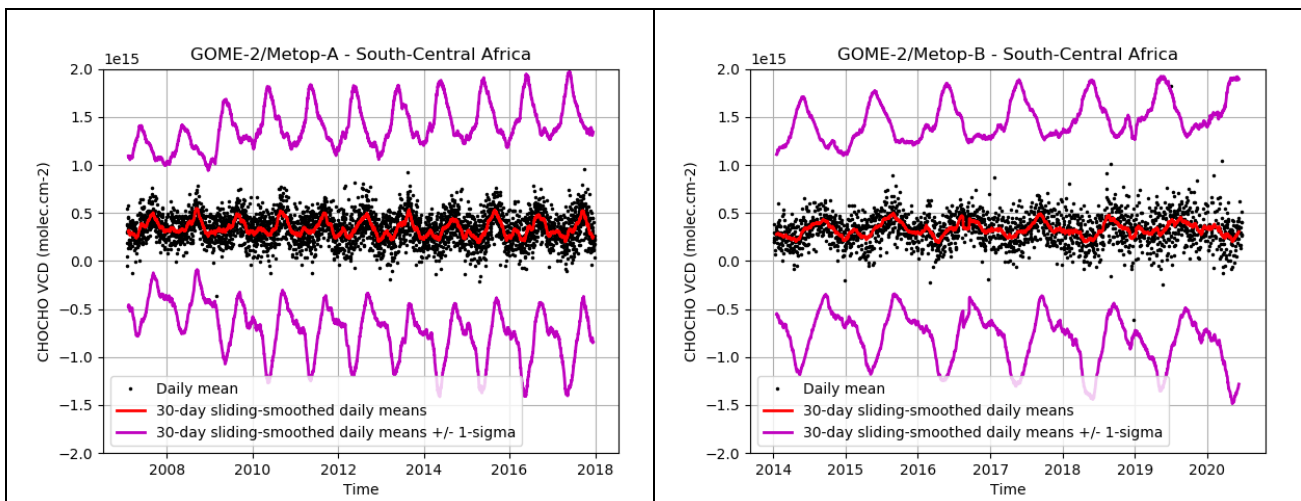


Figure B2: Time series of glyoxal vertical columns observations from GOME-2/Metop-A (left panel) and GOME-2/Metop-B (right panel) in a large region of South-Central Africa ([6°S-18°S; 13°E-30°E]). Daily averaged data are shown in black, the red curve corresponds to a 30-day sliding mean applied to those daily data, and the magenta lines show the mean daily signal +/- the daily standard deviation (1-sigma).

C. INTER-SATELLITE COMPARISONS

In this section, the glyoxal VCD data products generated from GOME-2A and GOME-2B are compared to scientific data products similarly retrieved from the Aura OMI and Sentinel-5p TROPOMI sensors (Lerot et al., 2020). To allow a visual assessment of the overall consistency of the various data sets, Figs C1 and C2 present global maps of long-term averaged VCDs from each sensors covering the four seasons. In each case, the available time-series were considered in the averaging process, to minimize the impact of the noise and display the systematic patterns of emissions.

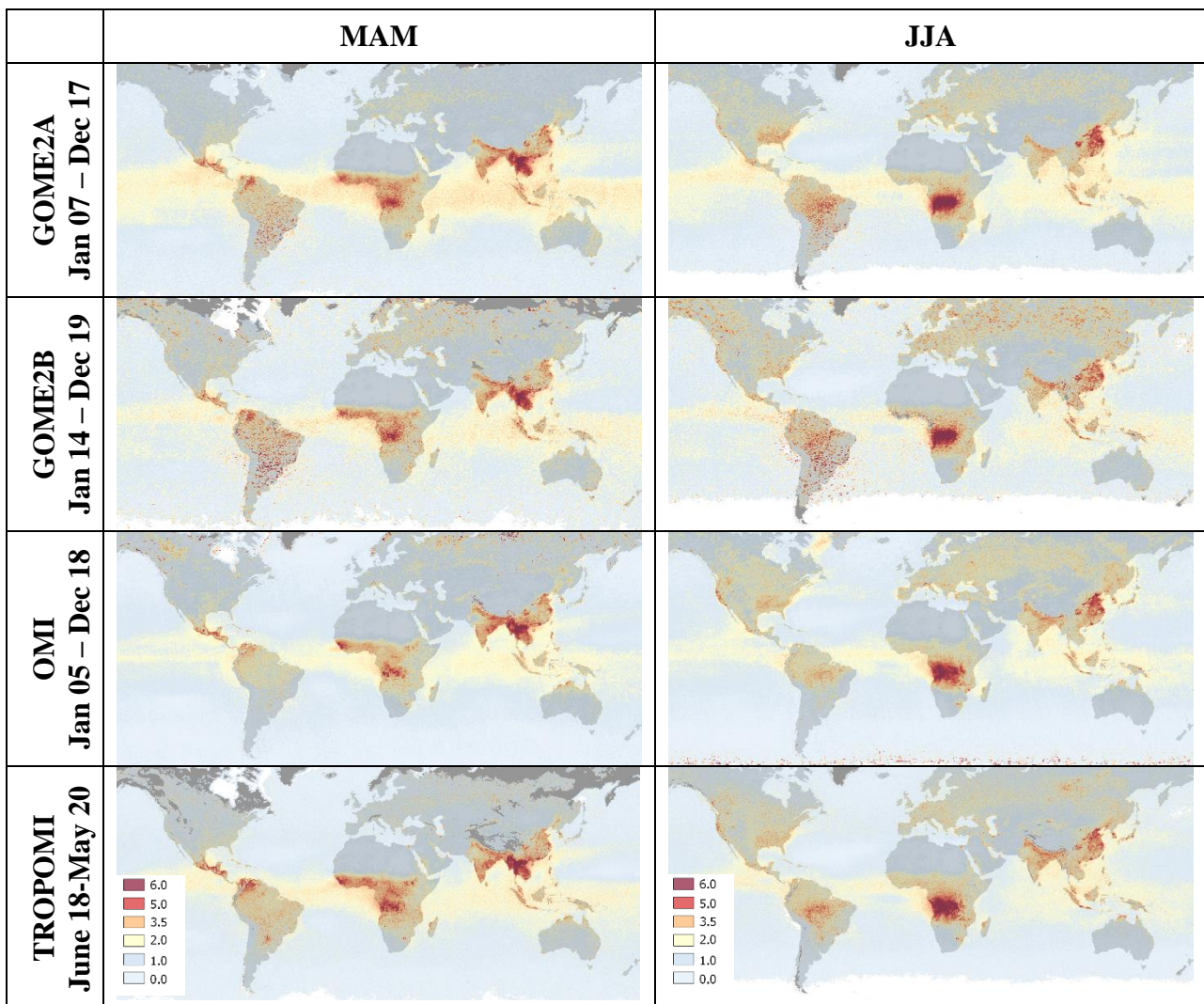


Figure C1: Comparison of long-term averaged global CHOCHO VCDs derived from GOME-2A, GOME-2B, OMI and TROPOMI sensors, for the March-April-May period (left panels) and the June-July-August period (right panels).

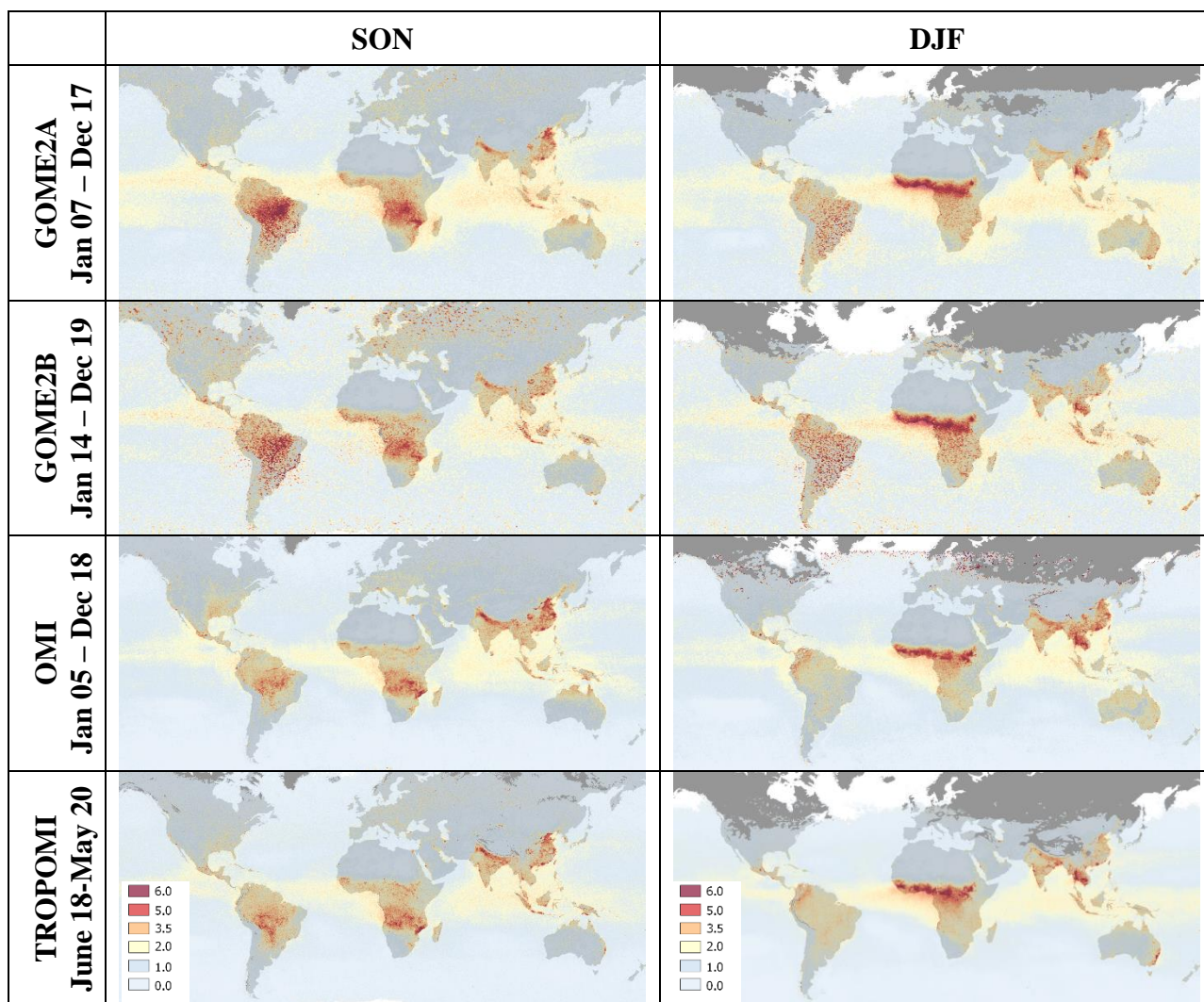


Figure C2: Comparison of long-term averaged global CHOCHO VCDs derived from GOME-2A, GOME-2B, OMI and TROPOMI sensors, for the September-October-November period (left panels) and the December-January-February period (right panels).

From the inspection of these figures, one can conclude that:

- All four instruments observe highly consistent glyoxal signal and variability in terms of spatial distribution and magnitude.
- Largest glyoxal columns are observed in tropical regions, where the biogenic emissions are important, and in regions with important fire events (e.g. Amazonia and Northern Africa in SON, Thailand/Indochina in MAM, Western US in August,...). At mid-latitude, the glyoxal columns follow the seasonal cycle of biogenic activity with maximum values during summer time. Localized hot spots of glyoxal are visible over megacities corresponding to strong anthropogenic emissions (e.g. Northern China Plain, Bangkok, Teheran, New Delhi, Sao Paulo,...)

- Periods covered by the four instruments differ in length and timing, which may explain differences in regions with variable emissions from one year to another. For example, high glyoxal columns are visible in eastern Australia in the 2-year period covered by the TROPOMI record. This signal mostly originates from intense fires that occurred in January 2020 and is therefore less important in the data sets derived from other satellites.

Fig. C3 displays the global distribution of CHOCHO absolute differences between GOME-2A and -B and OMI, based on a common period of one year. The upper plot shows the differences between GOME-2A and OMI for 2007, when the OMI global coverage was not yet impacted by the row anomaly (Schenkeveld et al., 2017). Differences are small, generally less than 1×10^{14} molec.cm⁻². Differences appear somewhat larger at southern oceanic high latitudes. This could be caused by a slightly different latitudinal dependence of the measured background glyoxal columns, but also by different the sampling caused by the different probing time of the two instruments. The diurnal variation of the glyoxal signal may also explain the larger differences observed over Amazonia and to a lesser extent over Africa.

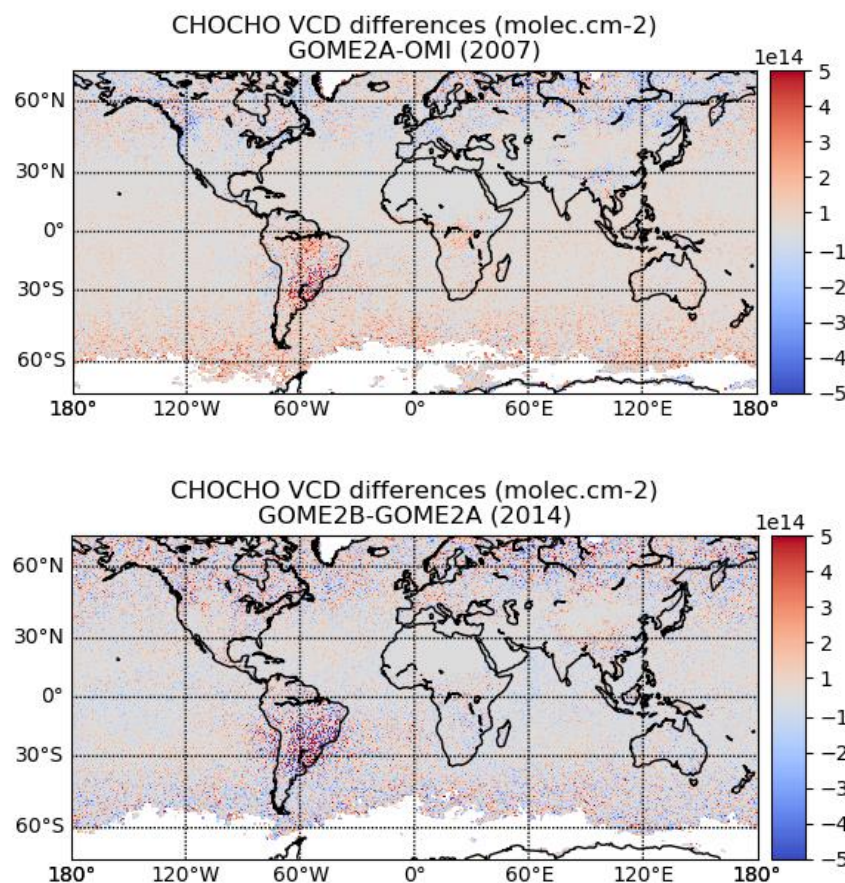


Figure C3: Global distribution of the CHOCHO absolute differences between respectively GOME-2A and OMI (upper plot) and GOME-2B and GOME-2A (lower plot), based on a common period of one year.

The lower plot of Fig. C3 explores the consistency between the two GOME-2 instruments, both flying at the same equator crossing times. As can be seen, differences are very small ($< 5 \times 10^{13}$ molec.cm⁻²) and most of the visible patterns seem to be randomly distributed.

To further investigate the time-dependence of the consistency between the different data sets, complete time-series of monthly median glyoxal columns in the regions shown in Fig. C4 are illustrated for the four satellite data sets in tropical regions (Fig. C5), Asia (Fig. C6) and mid-latitudes (Fig. C7). The error bars represent the estimated total errors associated to the retrievals. Right panels show climatological seasonalities for the four instruments based on different available time periods. In those panels, the error bars give an indication of the interannual variability. The mean scatter between those satellite products is indicated in each figure by the 2-sigma standard deviation.

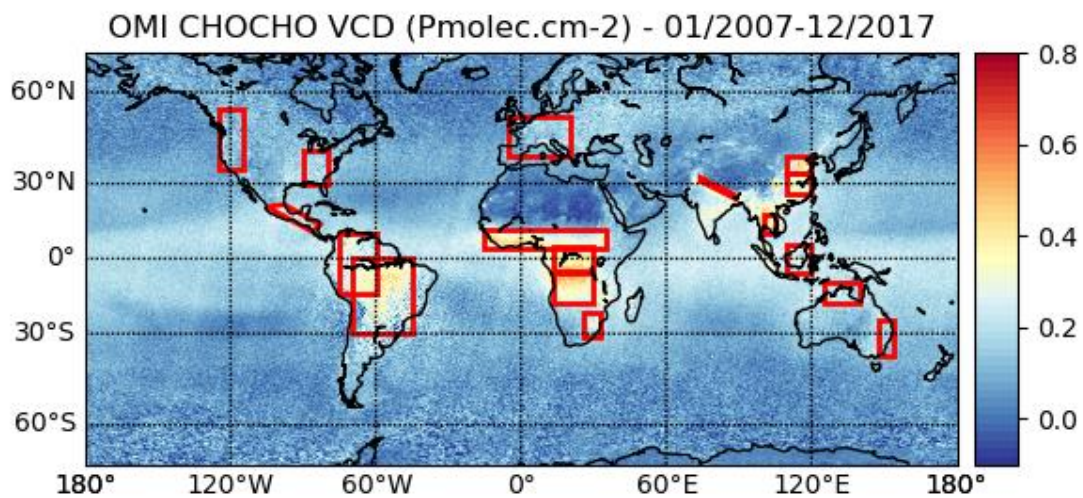
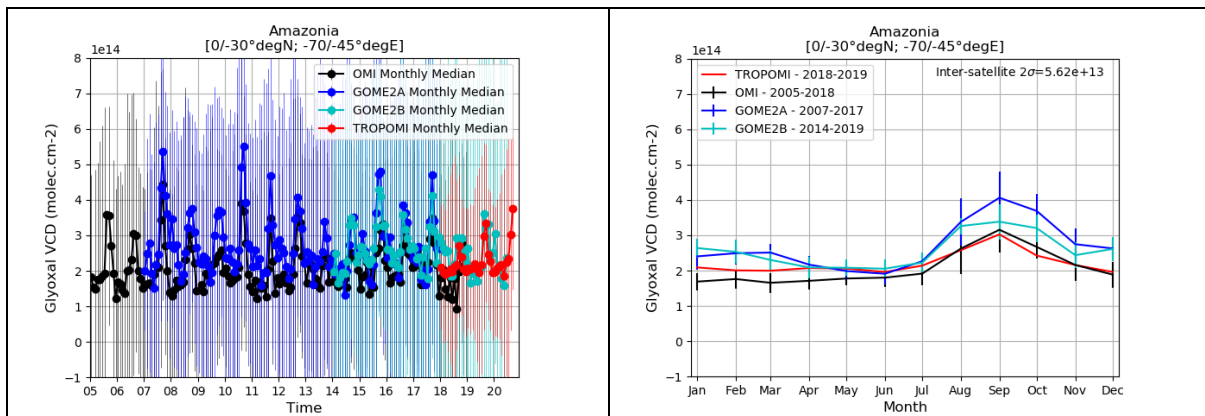
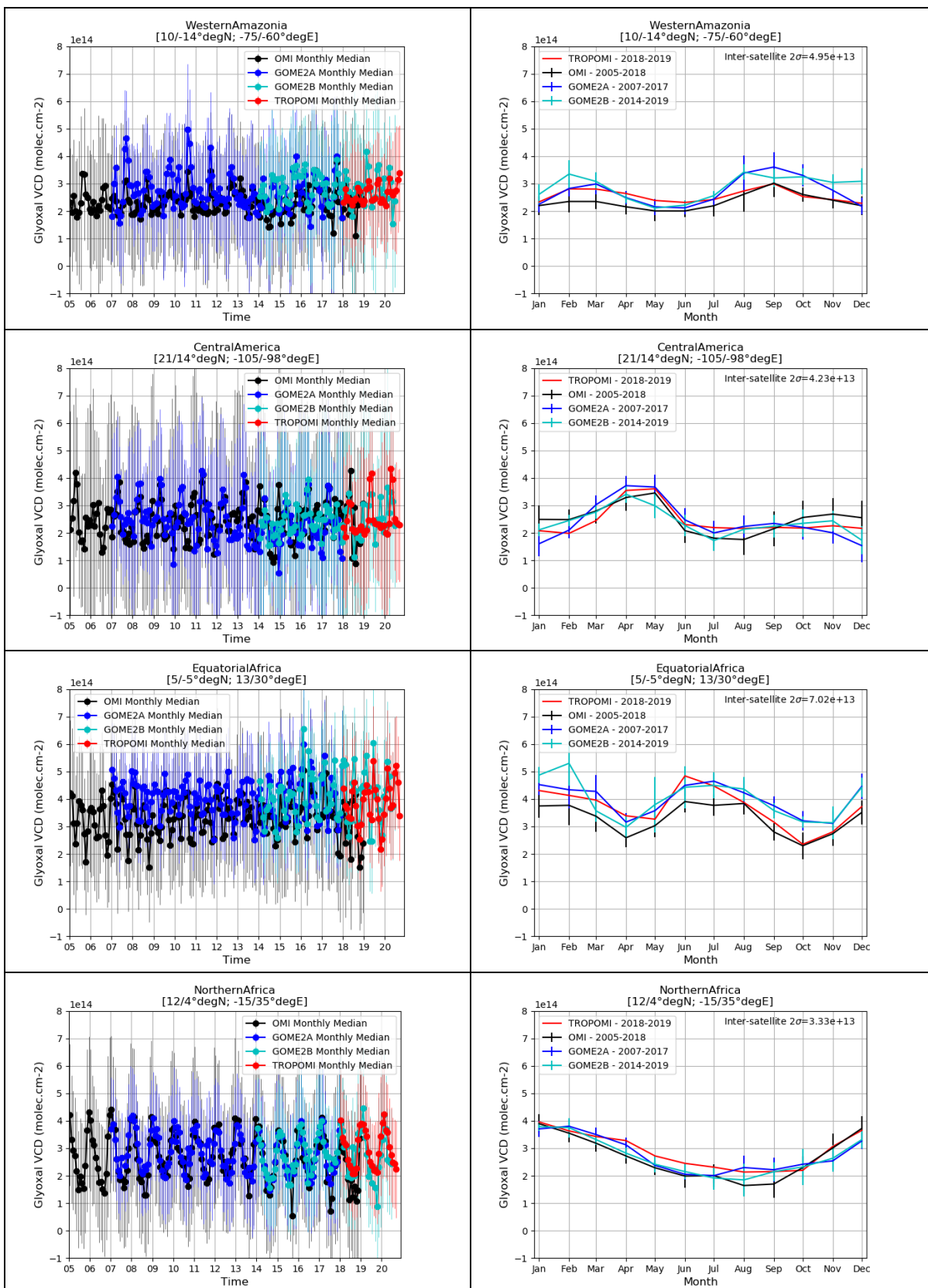


Figure C4: Long-term averaged map of OMI glyoxal VCDs, displaying the various reference regions selected for the analysis of time-series presented in the figures below. Each region corresponds to particular emissions.

Tropics





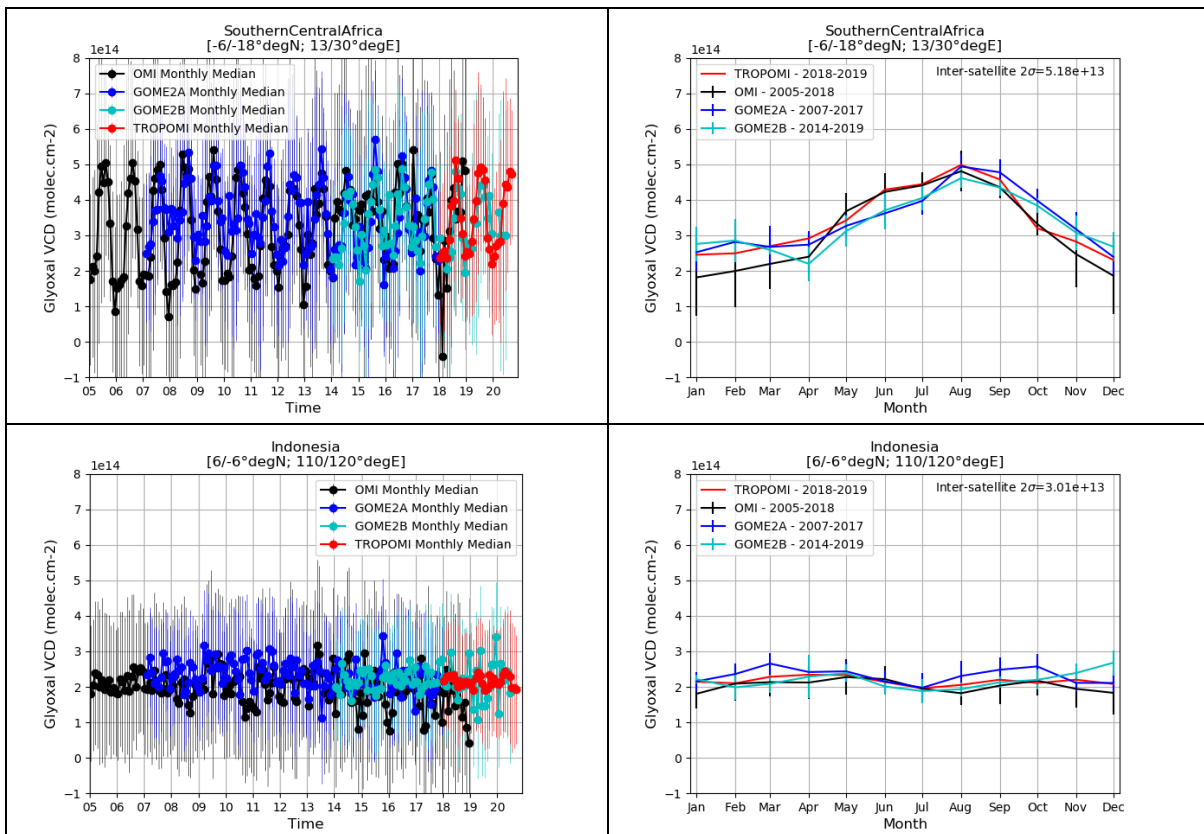


Figure C7: Time-series of monthly median glyoxal columns derived from the GOME-2A, GOME-2B, OMI and TROPOMI instruments, over seven different regions of the Tropics characterized by strong emissions of VOCs.

In the Tropics, the four data sets are relatively stable in time although a few outliers appear in the OMI data set after 2013-2014. All instruments observe similar seasonalities and columns in the same range of magnitude. The two GOME-2 data sets agree particularly well and seem to be slightly higher in Amazonia than the afternoon instruments, likely due to a real diurnal dependence.

The two regions defined in Amazonia show high inter-annual variability due to variable fire activities from a year to another. Glyoxal columns respond directly to this fire activity. Other regions display a more regular seasonal cycle, consistently seen by the four instruments. In equatorial Africa, OMI gives lower CHOCHO columns than the GOME-2 instruments. TROPOMI gives columns in better agreement with the GOME-2 instruments during the 1st part of the year and then agrees better with OMI. Note that the number of entire years available for TROPOMI is limited to two, which makes this climatological estimate uncertain.

Asia

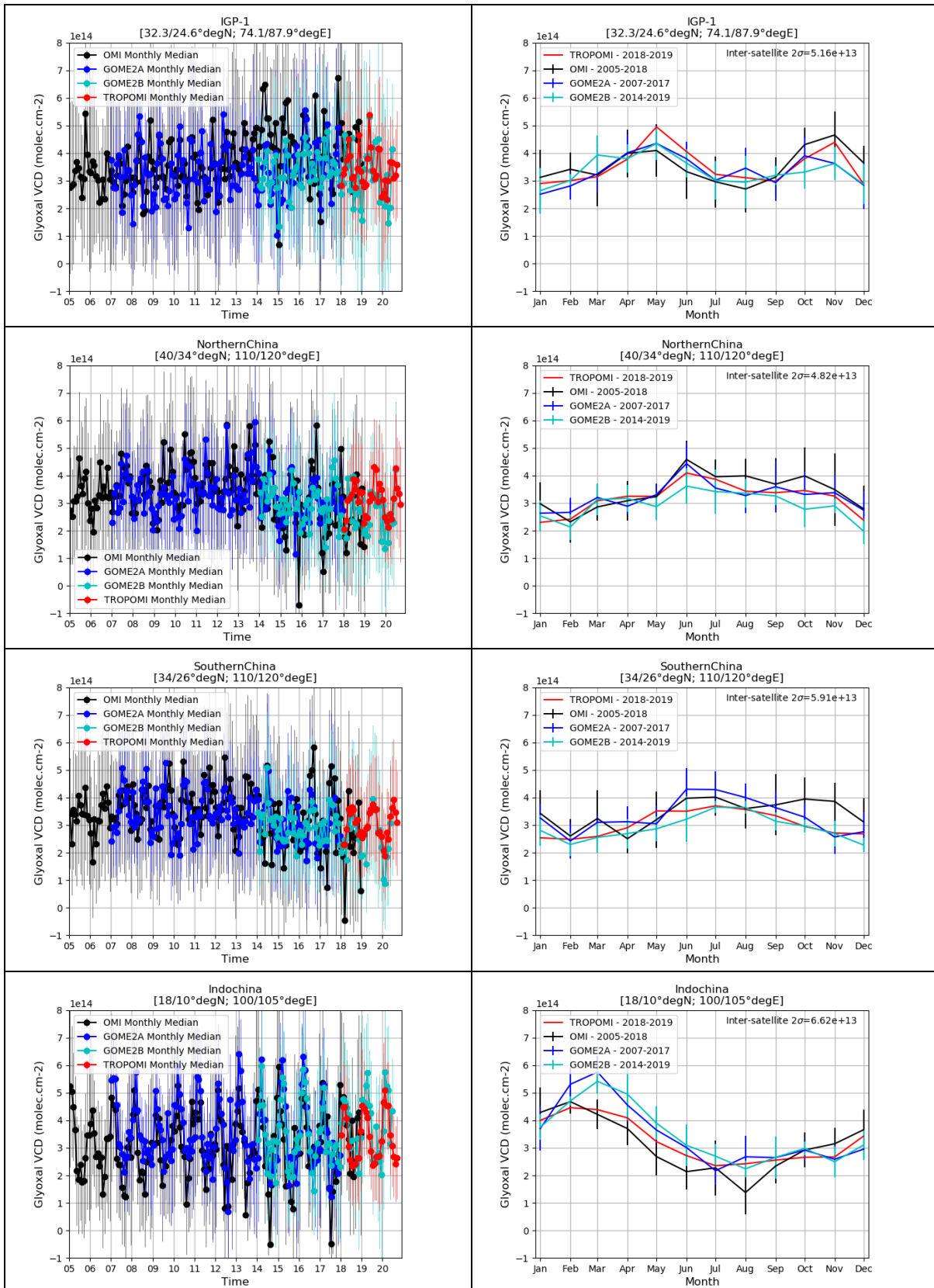
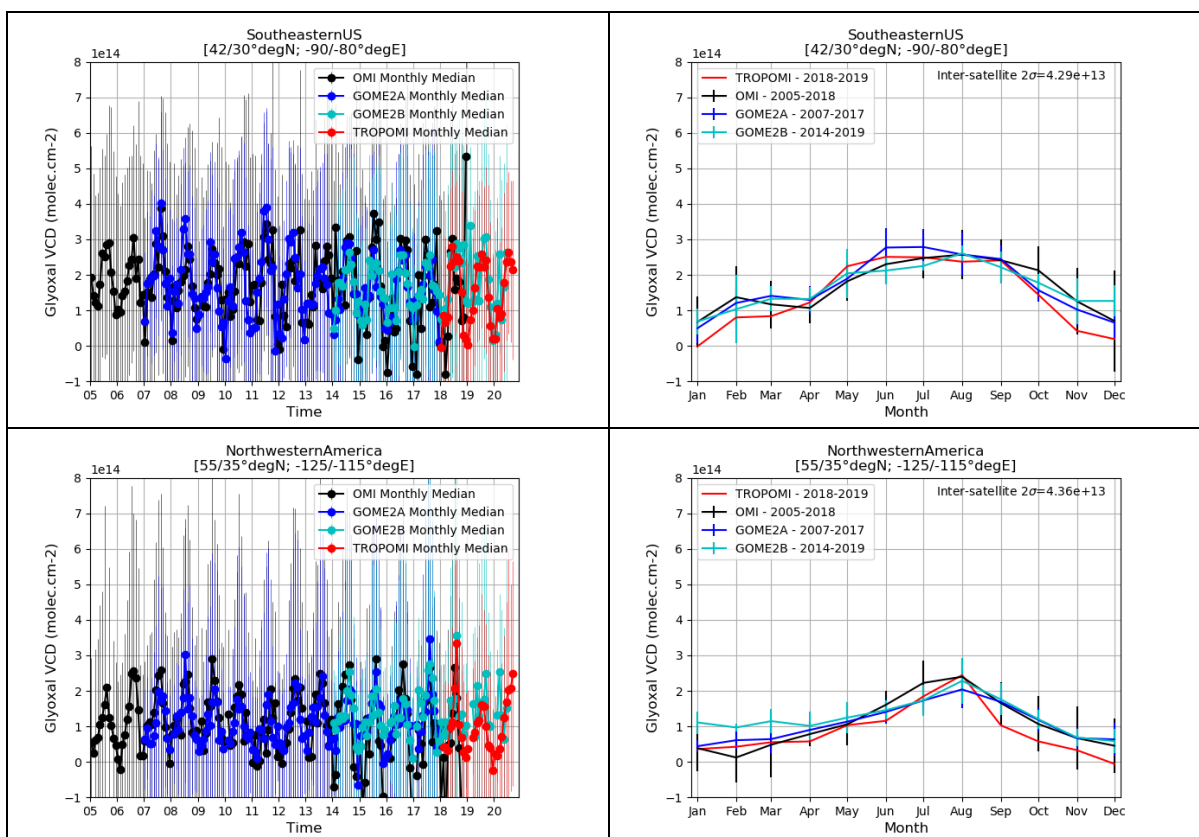


Figure C8: Time-series of monthly median glyoxal columns derived from the GOME-2A, GOME-2B, OMI and TROPOMI instruments, over four different regions in Asia characterized by strong emissions of VOCs.

In Asia (Fog. C8), the origin of the atmospheric glyoxal is manifold and depends strongly on the region and season. In addition to biogenic activities, of which the seasonal cycle amplitude depends on the latitude, large emissions due to fires may significantly contribute to the glyoxal concentrations. For example, in the Indo-Gangetic plains, there are typically two “fire” seasons in April/May and in October/November after the Monsoon, while in Indochina, a large fire season occurs around March. There is a large variability in the intensity of those fire events. Many regions are densely populated, causing large emissions due to human activities. This also leads to large glyoxal columns. For example, in China, they remain relatively large in winter, while biogenic emissions are low at that period of the year. Although less variable than emissions due to fires, anthropogenic emissions may also change in time.

Despite those variable emissions, the four data sets show a high level of consistency. In China, it seems that the glyoxal columns slightly increase until 2014 and then start to decrease. This behavior is visible in OMI, GOME-2A and GOME-2B. On the other hand, in India, while the OMI columns increase with time, this is not visible in any of the GOME-2 data sets. We therefore attribute this behavior to instabilities in the OMI record probably related to the evolution of the row anomaly (Schenkeveld et al., 2017). The latter also causes an increasing number of outliers in the OMI record.

Mid-Latitudes



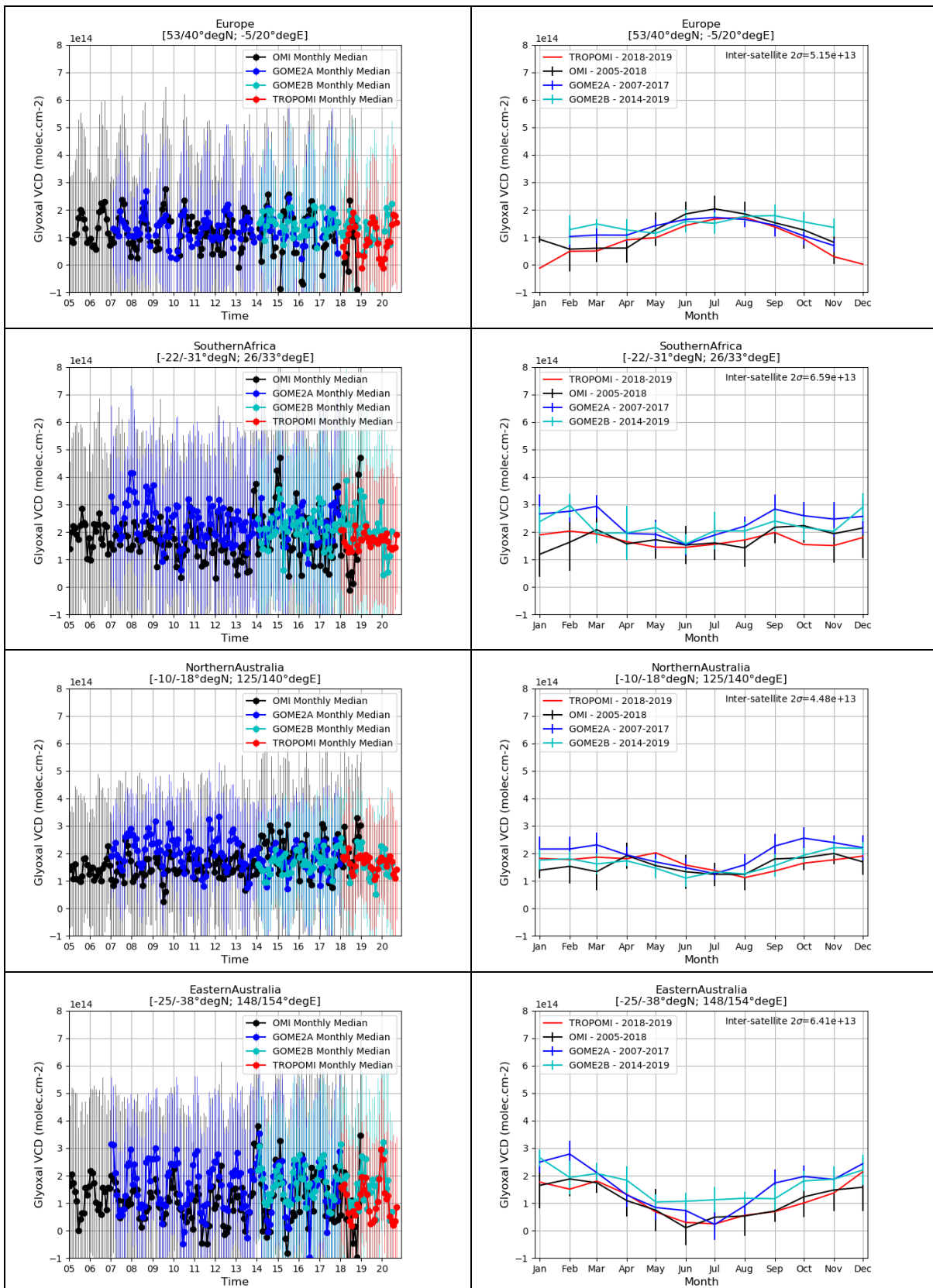


Figure C9: Time-series of monthly median glyoxal columns derived from the GOME-2A, GOME-2B, OMI and TROPOMI instruments, over six different mid-latitude regions in the Northern and Southern hemispheres.

At mid-latitudes (Fig. C9), the combination of the lower glyoxal concentrations and the lower sun elevation makes the retrievals more difficult. Although a small maximum is consistently observed during the local summertime, the level of consistency is somewhat poorer than in other regions. During winter, the sampling of the morning instrument may also differ significantly from the afternoon instruments as the SZA validity threshold is exceeded for lower latitudes.

The impact of the evolving row anomaly on the stability of the OMI data set is also the largest at such mid-latitudes. A systematic low bias appears from 2014 onwards during winter. Despite those more difficult conditions, the two GOME-2 instruments still provide reasonable and geophysical-sound glyoxal columns.

Figs. C10 and C11 summarize for all the regions investigated in this study the absolute and relative deviation of each of the four data sets with respect to their overall median values. The symbols represent the mean deviation considering all months of the year, while the error bars represent the full range of the monthly deviations. In Fig. C10, the requirements of 50% and 30% defined for polluted conditions were translated into absolute values considering a reference glyoxal column of 1.5×10^{14} molec.cm⁻². They are represented by the light and dark blue regions. Based on those inter-satellite comparisons, the specified accuracy requirements are clearly met.

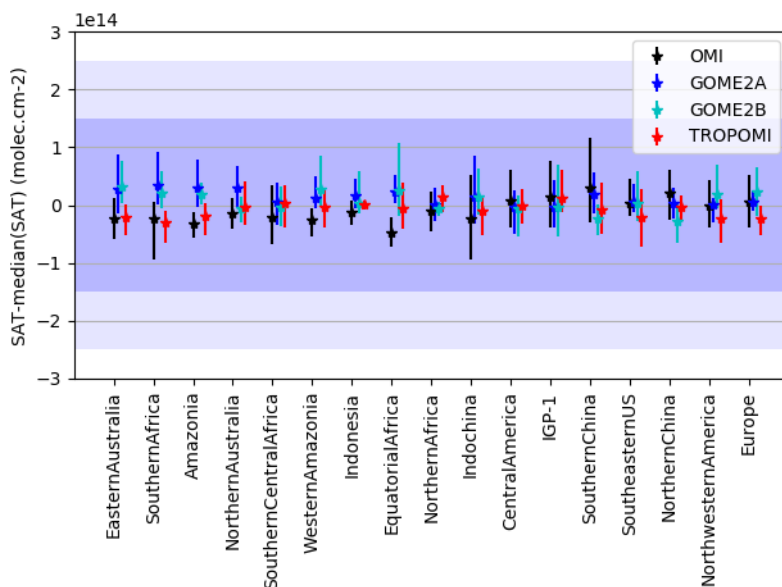


Figure C10: Absolute median deviations between glyoxal vertical columns in selected emission regions against their overall median value (see text).

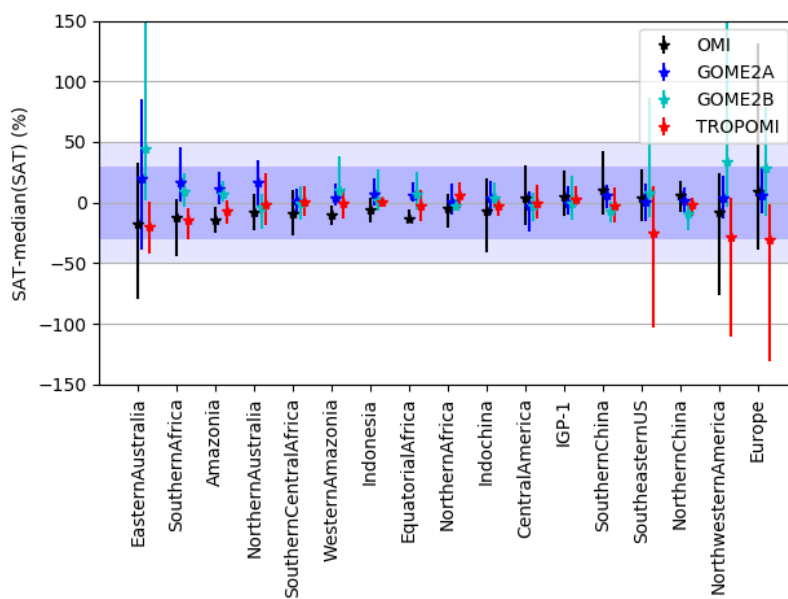


Figure C11: Same as Fig. C10, but in relative (percent) values.

D. COMPARISONS WITH GROUND-BASED MEASUREMENTS

D1. Ground-based MAX-DOAS data sets description

In this validation exercise, GOME-2A and GOME-2B CHOCHO vertical column densities (VCDs) are assessed through comparison to correlative observations from five MAX-DOAS instruments operated by BIRA-IASB (Xianghe and Uccle) and Chiba-University (Chiba University, Kasuga and Phimai). MAX-DOAS profiles are retrieved at BIRA-IASB stations using the bePRO Optimal Estimation-based profiling tool (Cl mer et al., 2010; Hendrick et al., 2014) while a profile parameterization approach (Irie et al., 2011), is used in the case of the Chiba University stations. Further information on the ground-based MAX-DOAS sets can be found in Table D1 and in the aforementioned references.

Table D1: MAX-DOAS CHOCHO datasets included in this validation exercise. OEM stands for Optimal Estimation Method and PP for Parametrized Profiling.

Station/Country (lat/long)	Station Type	Owner/ Group	Time Period	Instrument Type	Retrieval Type
Uccle/Belgium, (50.78° N, 4.35° E)	Urban	BIRA-IASB	02/2017-02/2020	Custom-built MAX-DOAS	VCD and profiles from OEM
Xianghe/China, (39.75° N, 116.96° E)	Sub- urban	BIRA-IASB	03/2010-08/2020	Custom-built MAX-DOAS	VCD and profiles from OEM
Chiba/Japan, (35.63°N, 140.10°E)	Urban	ChibaU	06/2012-04/2020	CHIBA-U MAX- DOAS	VCD and profiles from PP
Kasuga/Japan, (33.52°N, 130.48°E)	Sub- urban	ChibaU	12/2013-04/2020	CHIBA-U MAX- DOAS	VCD and profiles from PP
Phimai/Thailand, (15.18°N, 102.56°E)	Sub- urban	ChibaU	09/2014-12/2019	CHIBA-U MAX- DOAS	VCD and profiles from PP

Satellite CHOCHO VCD daily means are calculated using all pixels falling within a radius of 150 km around the stations. In order to allow direct comparison between GOME-2A, GOME-2B and MAX-DOAS observations, the difference in vertical sensitivity between both measurement types are taken into account by smoothing the MAX-DOAS CHOCHO profiles (x_{MAXDOAS}) with the satellite column averaging kernels (AK_{sat}) using the following equation:

$$VCD_{\text{MAXDOAS,smoothed}} = AK_{\text{sat}} * x_{\text{MAXDOAS}}$$

In practice, the smoothed MAX-DOAS CHOCHO VCDs ($VCD_{\text{MAXDOAS,smoothed}}$) are derived for each day by averaging retrieved MAX-DOAS profiles falling within the daily satellite overpass time ± 1.5 h and convolving the mean profile with the corresponding satellite column averaging kernel. If the first altitude level of the satellite averaging kernel is above the altitude of the station, the averaging kernel is extrapolated down to the altitude of the station.

D2. Comparison results

CHOCHO VCD time-series at the five stations included in this validation exercise are shown in Figs D1-D5. An overview of the mean absolute and relative biases and their corresponding standard deviations is given in Table D2.

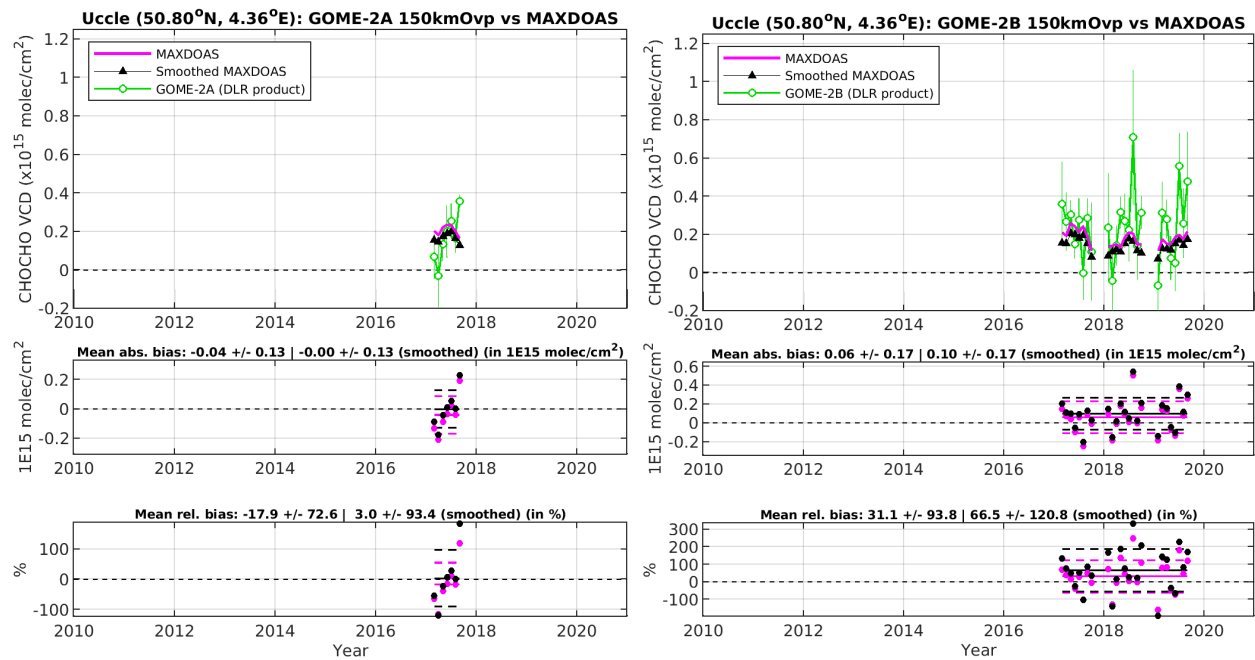


Figure D1: Comparison of GOME-2A (left plot) and GOME-2B (right plot) CHOCHO VCD monthly means with MAX-DOAS data at the Uccle station.

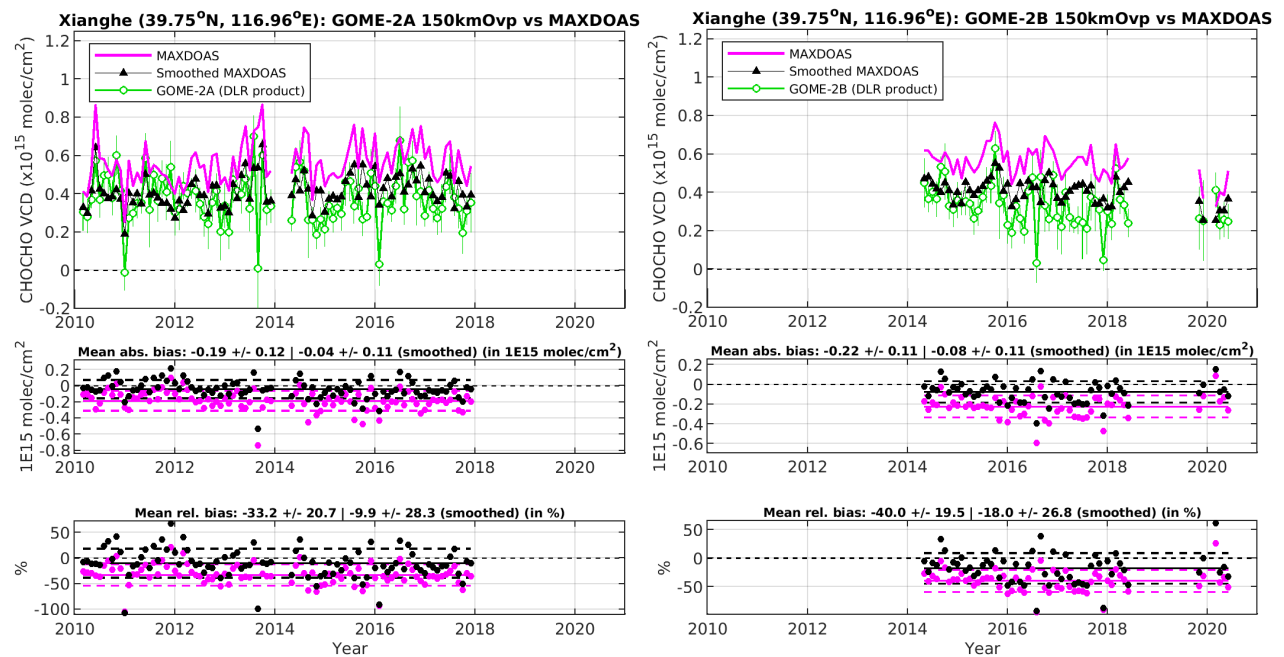


Figure D2: Same as Fig. D1 but for the Xianghe station.

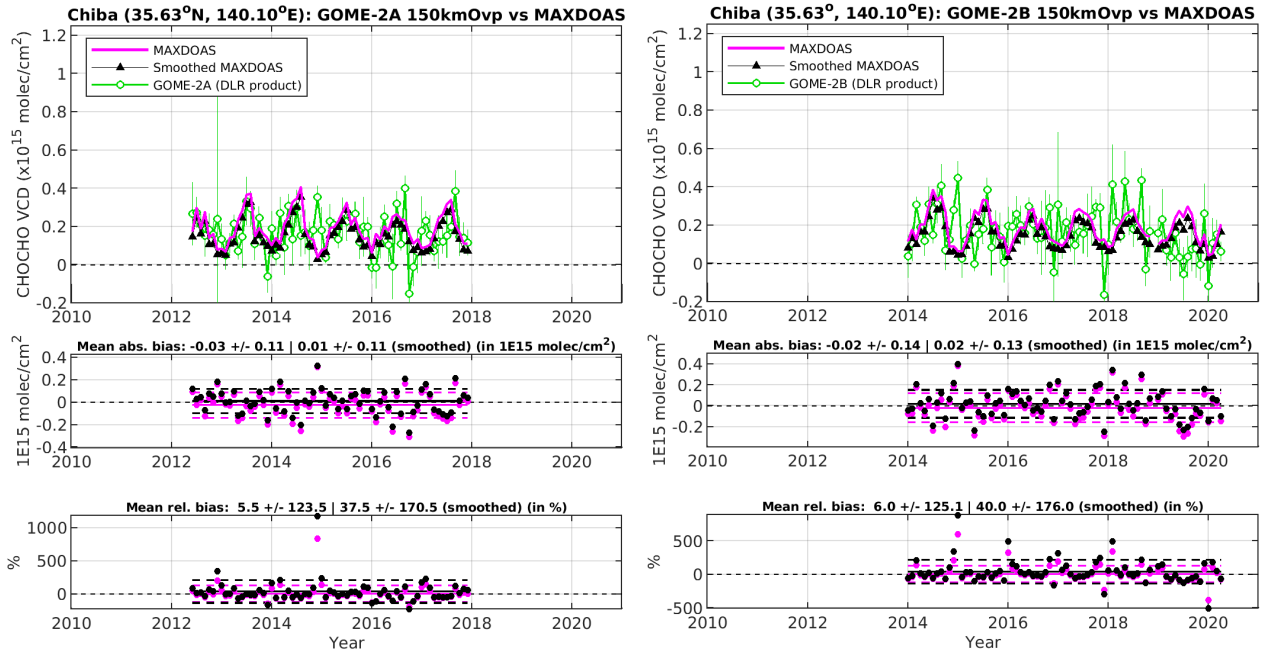


Figure D3: Same as Fig. D1 but for the Chiba station.

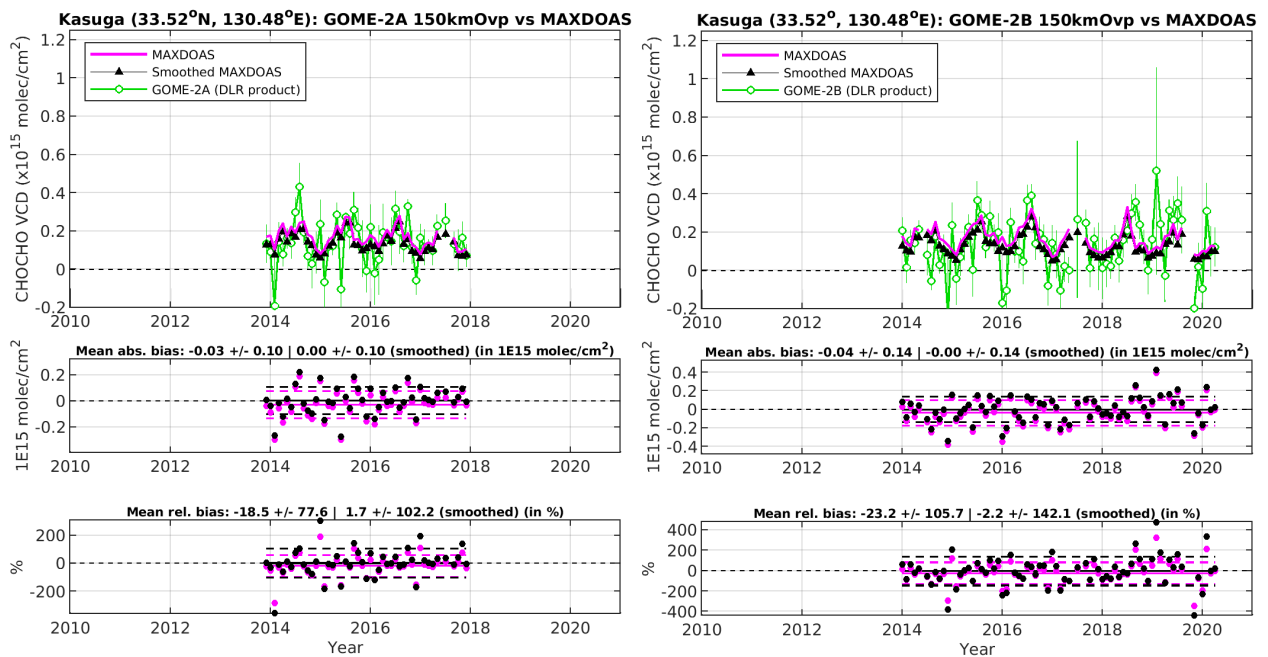


Figure D4: Same as Fig. D1 but for the Kasuga station.

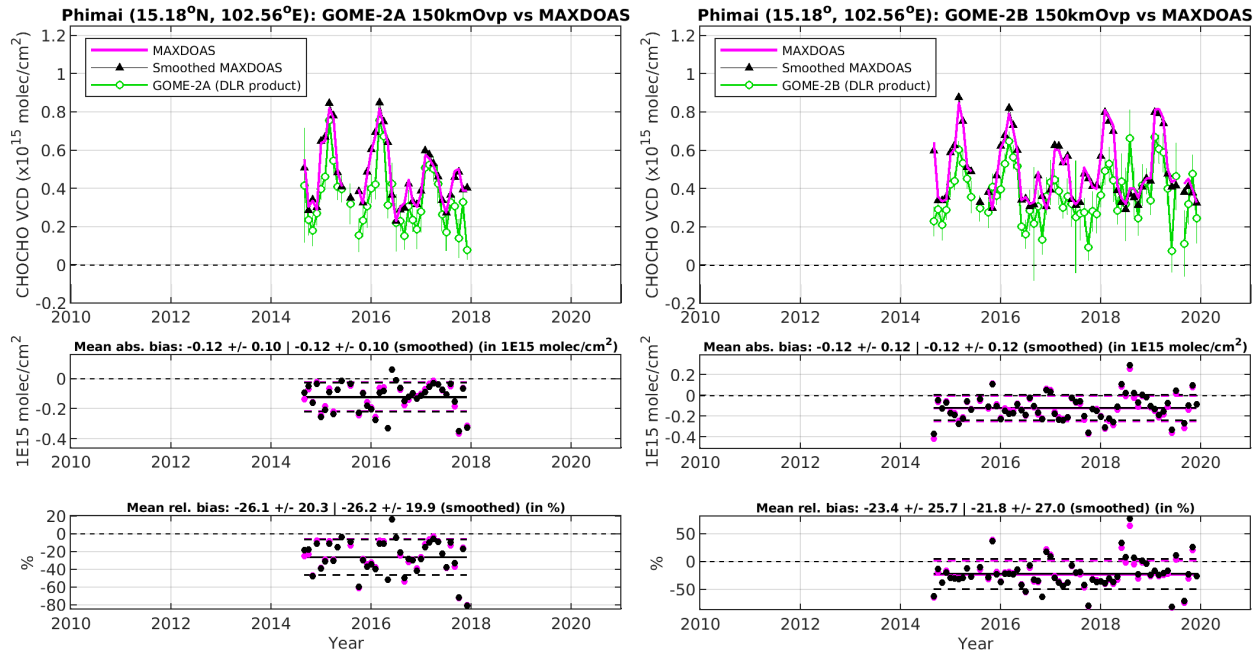


Figure D5: Same as Fig. D1 but for the Phimai station.

Table D2: Averaged absolute difference and standard deviation (AD and STDEV, in 10^{15} molec/cm²), relative difference and standard deviation (RD and STDEV, in %) between GOME-2A and GOME-2B CHOCHO VCDs and co-located MAX-DOAS data. Values between brackets correspond to comparison results when MAX-DOAS vertical profiles are smoothed with the satellite AVKs (see Sect. D.1).

	GOME-2A				GOME-2B			
	AD ($\times 10^{15}$)	STDEV ($\times 10^{15}$)	RD (%)	STDEV (%)	AD ($\times 10^{15}$)	STDEV ($\times 10^{15}$)	RD (%)	STDEV (%)
ccle	-0.04 [-0.00]	0.13 [0.13]	-17.9 [3.0]	72.6 [93.4]	0.06 [0.10]	0.17 [0.17]	31.1 [66.5]	93.8 [120.8]
Xianghe	-0.19 [-0.04]	0.12 [0.11]	-33.2 [-9.9]	20.1 [28.3]	-0.22 [-0.08]	0.11 [0.11]	-40.0 [-18.0]	19.5 [26.8]
Chiba	-0.03 [0.01]	0.11 [0.11]	5.5 [37.5]	123.5 [170.5]	-0.02 [0.02]	0.14 [0.13]	6.0 [40.0]	125.1 [176.0]
Kasuga	-0.03 [0.00]	0.10 [0.10]	-18.5 [1.7]	77.6 [102.2]	-0.04 [-0.00]	0.14 [0.14]	-23.2 [-2.2]	105.7 [142.1]
Phimai	-0.12 [-0.12]	0.10 [0.10]	-26.1 [-26.2]	20.3 [19.9]	-0.12 [-0.12]	0.12 [0.12]	-23.4 [-21.8]	25.7 [27.0]

The mean relative bias between GOME-2A and MAX-DOAS VCDs at the five stations ranges between -33.2% and +5.5%, which is within the accuracy requirement of 50%. The mean bias between GOME-2B and MAX-DOAS data is comprised between -40.0% and +31.1%, i.e. also within the required accuracy requirements.

Except for Phimai, the difference between GOME-2 and MAX-DOAS data is slightly larger for GOME-2B than for GOME-2A. The standard deviations are also larger for GOME-2B, except in Xianghe. This suggests that GOME-2B VCDs are slightly noisier than GOME-2A VCDs.

The smoothing of the MAX-DOAS vertical profiles with satellite averaging kernels generally improves the agreement between both data sets, except for GOME-2B over Uccle and GOME-2A and B over Chiba.

The annual cycles corresponding to the time-series presented in Figs D1-D5 are displayed in Figs D6-D10.

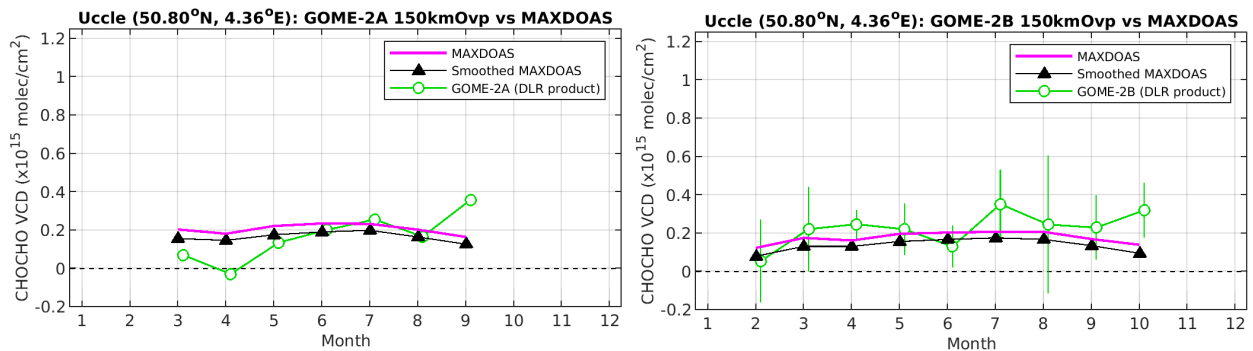


Figure D6: GOME-2A (left plot) and GOME-2B (right plot) CHOCHO VCD annual cycles compared to MAX-DOAS data at the Uccle station.

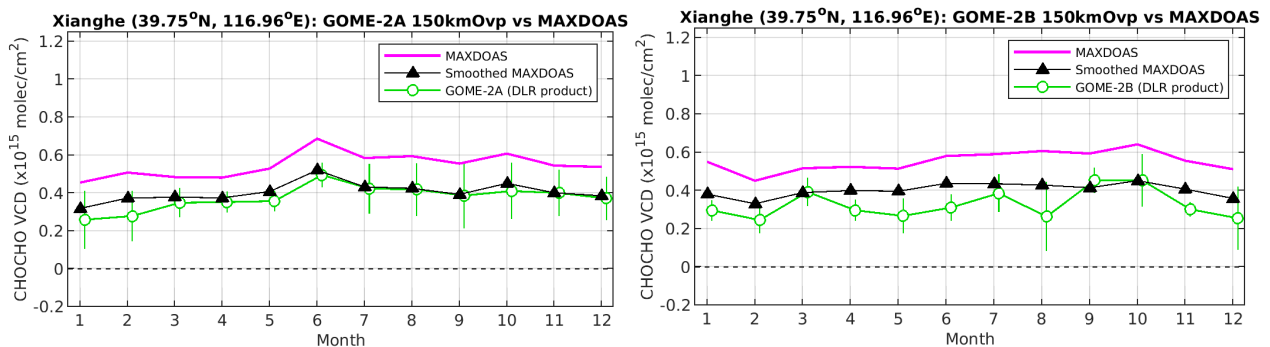


Figure D7: Same as Fig. D6 but for the Xianghe station.

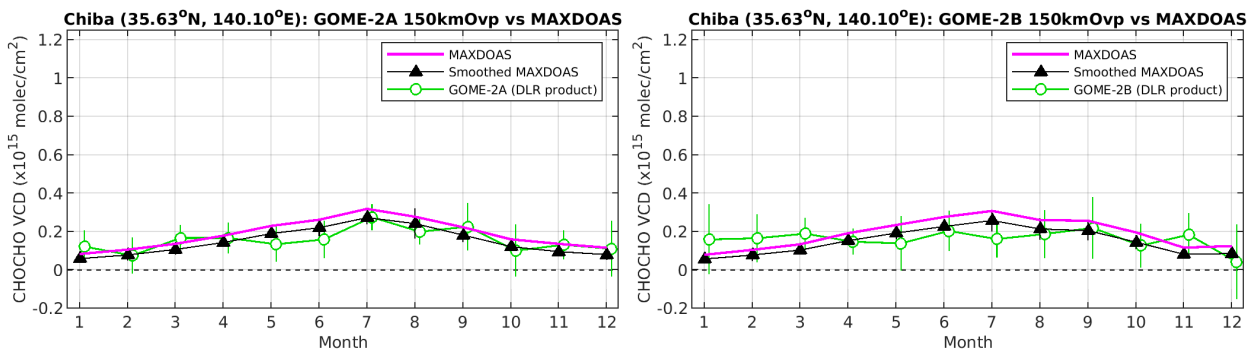


Figure D8: Same as Fig. D6 but for the Chiba station.

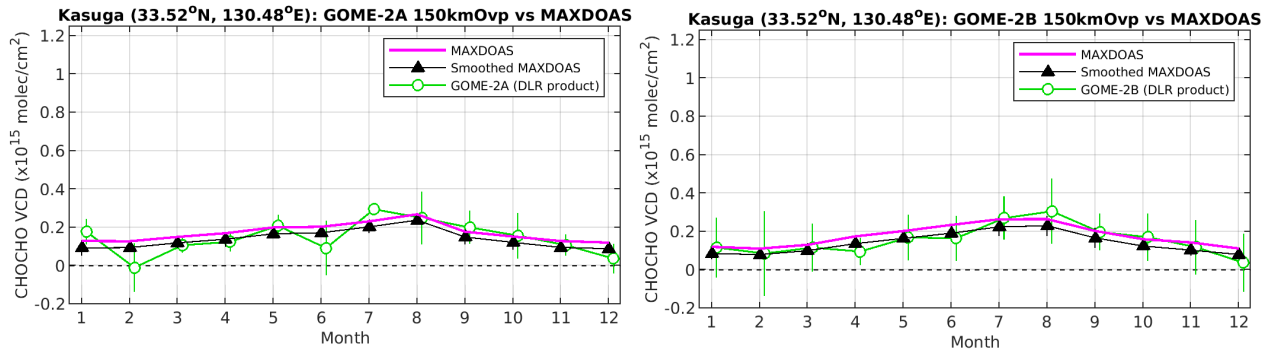


Figure D9: Same as Fig. D6 but for the Kasuga station.

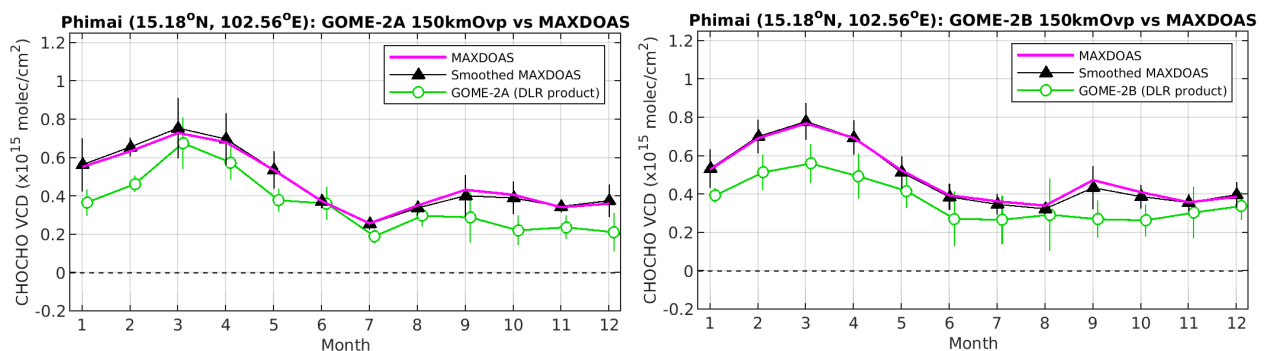


Figure D10: Same as Fig. D6 but for the Phimai station.

The annual cycle of the MAX-DOAS CHOCHO VCDs is generally well captured by the satellite observations, except in Uccle where larger discrepancies are found. The latter feature could be related to the poorer comparison statistics at the Uccle station compared to the other stations. The double peak structure with maximum VCD values in March and September observed in Phimai with both satellite and ground-based data is caused by agricultural fires occurring during these periods of the year in this region.

Results indicate that satellite data tend to underestimate MAX-DOAS VCDs, especially in Xianghe and Phimai (see also Table D2). The quantitative agreement between satellite and MAX-DOAS seasonal cycles is however improved when MAX-DOAS vertical profiles are smoothed with the satellite averaging kernels. This is especially visible in Xianghe. Note that the larger impact of the smoothing at the BIRA-IASB stations (Xianghe and Uccle) might be due to the different MAX-DOAS retrieval algorithms used by the BIRA and Chiba teams. In particular the use of thinner retrieval altitude grid layers at the BIRA stations (layer thicknesses of 200 m in comparison to 1 km for Chiba) may explain the observed different behaviors.

E. CONCLUSIONS

This document reports on the validation of AC-SAF GOME-2A and GOME-B glyoxal column data products retrieved at DLR with versions 1.0 of the G2_L2_GLY processor, using level-1 data based on level-0-to-1B processor version 6.3. GOME-2 Glyoxal column data were compared to satellite correlative data from the Aura OMI and Sentinel-5p TROPOMI instruments, as well as with ground-based MAX-DOAS data. Those comparisons rely on data averaged in space and time, which are necessary to reduce the large random error component on individual measurements and allow for the identification of possible systematic biases in the products.

Main conclusions from the inter-satellite comparisons are:

1. GOME-2A and GOME-2B glyoxal VCDs are in general good agreement with both OMI and TROPOMI. All instruments observe similar seasonalities and VCDs are in the same range of magnitude. The two GOME-2 data sets agree particularly well. In some regions, a systematic difference is found between mid-morning GOME-2 and early afternoon OMI and TROPOMI data, which is likely to be due to actual diurnal variation effects.
2. An analysis of the time-series of data covering the complete lifetime of GOME-2A and GOME-2B show excellent stability in comparison with the reference OMI and TROPOMI data sets.
3. At mid-latitudes, the combination of the lower glyoxal concentrations and the lower sun elevation makes the retrievals more difficult, however even under these conditions the two GOME-2 instruments still provide reasonable and geophysically-sound glyoxal columns.
4. Considering all emission regions investigated in the study, GOME-2A and GOME-B glyoxal VCDs agree with correlative OMI and TROPOMI data within 1.5×10^{14} molec.cm⁻², corresponding to about 30% of median values. On this basis, we conclude that the GOME-2A and GOME-2B glyoxal products meet the optimum accuracy requirements of 30 % for polluted conditions.

The comparisons with ground-based MAX-DOAS measurements available at five stations lead to the following conclusions:

1. The mean relative bias between GOME-2A and MAX-DOAS VCDs at the five stations ranges between -33.2% and +5.5%, which is within the target accuracy requirement of 50% and close to the optimum requirement of 30%.
2. The mean bias between GOME-2B and MAX-DOAS data is comprised between -40.0% and +31.1%, i.e. also within the target accuracy requirements.
3. The difference between GOME-2 and MAX-DOAS data is slightly larger for GOME-2B than for GOME-2A. The standard deviations are also larger for GOME-2B, except in Xianghe, which suggests that GOME-2B data are slightly noisier than GOME-2A ones.
4. Results indicate that satellite data tend to underestimate MAX-DOAS VCDs at some of the stations. This underestimation can be mitigated to some extent by applying the satellite averaging kernels to the ground-based MAX-DOAS profiles.
5. Comparison with more MAX-DOAS data sets would be needed to assess more firmly the reported difference. Ideally, this analysis should be based on harmonized MAX-DOAS data sets, e.g. based on a common data processing as currently developed within the ESA FRM4DOAS project.

F. REFERENCES

G.1. Applicable documents

- [ATBD] Algorithm Theoretical Basis Document - GOME-2 Glyoxal column product, Valks P., Hao, N., and Lerot, C., SAF/AC/DLR/ATBD/GLY/01, Iss. 1/B, 2 December 2020.
- [PUM] Products User Manual – GOME-2 Glyoxal column product, Valks. P., SAF/AC/DLR/PUM/GLY/01, Iss. 1/A, 2 December 2020.
- [PRD] Service Specification Document, SAF/AC/FMI/RQ/SESP/001/issue 1.3, Hovila, J., Hassinen, S., 17 June 2019, https://acsaf.org/docs/AC_SAF_Service_Specification.pdf
- [VIM] Joint Committee for Guides in Metrology (JCGM/WG 2) 200:2008 & ISO/IEC Guide 99-12:2007, International Vocabulary of Metrology – Basic and General Concepts and Associated Terms (VIM), <http://www.bipm.org/en/publications/guides/vim.html>
- [GUM] Joint Committee for Guides in Metrology (JCGM/WG 1) 100:2008, Evaluation of measurement data – Guide to the expression of uncertainty in a measurement (GUM), http://www.bipm.org/utis/common/documents/jcgm/JCGM_100_2008_E.pdf

G.2. Reference

G.2.1 Peer-reviewed articles

- Beirle, S., Lampel, J., Lerot, C., Sihler, H., and Wagner, T.: Parameterizing the instrumental spectral response function and its changes by a super-Gaussian and its derivatives, *Atmos. Meas. Tech.*, 10, 581–598, <https://doi.org/10.5194/amt-10-581-2017>, 2017.
- Chance, K. V. and Spurr, R. J. D.: Ring effect studies: Rayleigh scattering, including molecular parameters for rotational Raman scattering, and the Fraunhofer spectrum, *Appl. Opt.*, 36(21), 5224, [doi:10.1364/ao.36.005224](https://doi.org/10.1364/ao.36.005224), 1997.
- Clémer, K., Van Roozendael, M., Fayt, C., Hendrick, F., Hermans, C., Pinardi, G., Spurr, R., Wang, P. and De Mazière, M.: Multiple wavelength retrieval of tropospheric aerosol optical properties from MAX-DOAS measurements in Beijing, *Atmos. Meas. Tech.*, 3, 863–878, [doi:10.5194/amt-3-863-352010](https://doi.org/10.5194/amt-3-863-352010), 2010.
- EUMETSAT (2011), GOME-2 Products Guide, Ref.: EUM/OPS-EPS/MAN/07/0445, Issue: v3, Date: 17 Mar 2011.
- Hendrick, F., Müller, J.-F., Clémer, K., Wang, P., De Mazière, M., Fayt, C., Gielen, C., Hermans, C., Ma, J. Z., Pinardi, G., Stavrou, T., Vlemmix, T. and Van Roozendael, M.: Four years of ground-based MAX-DOAS observations of HONO and NO₂ in the Beijing area, *Atmos. Chem. Phys.*, 14(2), 765–781, [doi:10.5194/acp-14-30765-2014](https://doi.org/10.5194/acp-14-30765-2014), 2014.
- Irie, H., Takashima, H., Kanaya, Y., Boersma, K. F., Gast, L., Wittrock, F., Brunner, D., Zhou, Y. and Van Roozendael, M.: Eight-component retrievals from ground-based MAX-DOAS observations, *Atmos. Meas. Tech.*, 4(1), 1027–1044, [doi:10.5194/amtd-4-639-2011](https://doi.org/10.5194/amtd-4-639-2011), 2011.
- Kleipool, Q. L., Dobber, M. R., de Haan, J. F. and Levelt, P. F.: Earth surface reflectance climatology from 3 years of OMI data, *J. Geophys. Res.*, 113(D18), D18308, [doi:10.1029/2008JD010290](https://doi.org/10.1029/2008JD010290), 2008.

- Lerot, C., Stavrakou, T., De Smedt, I., Müller, J.-F., & Van Roozendael, M. (2010). Glyoxal vertical columns from GOME-2 backscattered light measurements and comparisons with a global model. *Atmos. Chem. Phys.*, 10(24), 12059–12072. <https://doi.org/10.5194/acp-10-12059-2010>.
- Lerot, C., T. Stavrakou, M. Van Roozendael, L. M.A. Alvarado, A. Richter, Algorithm Theoretical Baseline Document, ESA Sentinel-5p + Innovation - Theme 1: CHOCHO, GLYoxal Retrievals from TROPOMI (GLYRETRO), S5p+I_CHOCHO_BIRA_ATBD, 5.10.2020.
- Mason, J. D., Cone, M. T. and Fry, E. S.: Ultraviolet (250–550 nm) absorption spectrum of pure water, *Appl. Opt.*, 55(25), 7163, doi:10.1364/AO.55.007163, 2016.
- Richter, A., and J. Burrows (2002), Tropospheric NO₂ from GOME measurements, *Adv. Space Res.*, 29, 1673-1683.
- Rothman, L. S., Gordon, I. E., Babikov, Y., Barbe, A., Chris Benner, D., Bernath, P. F., Birk, M., Bizzocchi, L., Boudon, V., Brown, L. R., Campargue, A., Chance, K., Cohen, E. A., Coudert, L. H., Devi, V. M., Drouin, B. J., Fayt, A., Flaud, J. M., Gamache, R. R., Harrison, J. J., Hartmann, J. M., Hill, C., Hodges, J. T., Jacquemart, D., Jolly, A., Lamouroux, J., Le Roy, R. J., Li, G., Long, D. A., Lyulin, O. M., Mackie, C. J., Massie, S. T., Mikhailenko, S., Müller, H. S. P., Naumenko, O. V., Nikitin, A. V., Orphal, J., Perevalov, V., Perrin, A., Polovtseva, E. R., Richard, C., Smith, M. A. H., Starikova, E., Sung, K., Tashkun, S., Tennyson, J., Toon, G. C., Tyuterev, V. G. and Wagner, G.: The HITRAN2012 molecular spectroscopic database, *J. Quant. Spectrosc. Radiat. Transf.*, 130, 4–50, doi:10.1016/j.jqsrt.2013.07.002, 2013.
- Schenkeveld, V. M. E., Jaross, G., Marchenko, S., Haffner, D., Kleipool, Q. L., Rozemeijer, N. C., Veefkind, J. P., and Levelt, P. F.: In-flight performance of the Ozone Monitoring Instrument, *Atmos. Meas. Tech.*, 10, 1957–1986, <https://doi.org/10.5194/amt-10-1957-2017>, 2017.
- Serdyuchenko, A., Gorshlev, V., Weber, M., Chehade, W. and Burrows, J. P.: High spectral resolution ozone absorption cross-sections – Part 2: Temperature dependence, *Atmos. Meas. Tech.*, 7(2), 625– 636, doi:10.5194/amt-7-625-2014, 2014.
- Siddans, R., B.J. Kerridge, B.G. Latter, J. Smeets and G. Otter (2006), Analysis of GOME-2 Slit function measurements, Algorithm Theoretical Basis Document, EUM/CO/04/1298/RM.
- Siddans, R., Kerridge, B.J., Latter, B. G., Smeets, J., Otter, G. (2012): Analysis of GOME-2 Slit function Measurements Algorithm Theoretical Basis Document, Eumetsat Contract No. EUM/CO/04/1298/RM.
- Stavrakou, T., Muller, J.-F., De Smedt, I., Van Roozendael, M., Kanakidou, M., Vrekoussis, M., Wittrock, F., Richter, A., and Burrows, J. P.(2009): The continental source of glyoxal estimated by the synergistic use of spaceborne measurements and inverse modelling, *Atmos. Chem. Phys.*, 9, 8431–8446, doi:10.5194/acp-9-8431-2009.
- Thalman, R. and Volkamer, R.: Temperature dependent absorption cross-sections of O₂–O₂ collision pairs between 340 and 630 nm and at atmospherically relevant pressure, *Phys. Chem. Chem. Phys.*, 15(37), 15371, doi:10.1039/c3cp50968k, 2013.
- Valks, P., et al., (2019), Algorithm Theoretical Basis Document for GOME-2 Total Column Products of Ozone, NO₂, BrO, HCHO, SO₂, H₂O, OClO and Cloud Properties (GDP 4.9 for O3M-SAF OTO and NTO), SAF/AC/DLR/ATBD/01, issue 3/B, 11.11.2019.
- Vandaele, A. C., Hermans, C., Simon, P. C., Carleer, M., Colin, R., Fally, S., Mérienne, M. F., Jenouvrier, A. and Coquart, B.: Measurements of the NO₂ absorption cross-section from 42 000 cm⁻¹ to 10 000 cm⁻¹ (238–1000 nm) at 220 K and 294 K, *J. Quant. Spectrosc. Radiat. Transf.*, 59(3–5), 171–184, doi:10.1016/S0022-4073(97)00168-4, 1998.
- Volkamer, R., Spietz, P., Burrows, J. and Platt, U.: High-resolution absorption cross-section of glyoxal in the UV–vis and IR spectral ranges, *J. Photochem. Photobiol. A Chem.*, 172(1), 35–46 [online] Available from:

[http://www.colorado.edu/chemistry/volkamer/publications/articles/Volkamer_etal_\(2005\)_HR_cross_section_glyoxal.pdf](http://www.colorado.edu/chemistry/volkamer/publications/articles/Volkamer_etal_(2005)_HR_cross_section_glyoxal.pdf), 2005.

- Volkamer, R., Baidar, S., Campos, T. L., Coburn, S., DiGangi, J. P., Dix, B., Eloranta, E. W., Koenig, T. K., Morley, B., Ortega, I., Pierce, B. R., Reeves, M., Sinreich, R., Wang, S., Zondlo, M. A. and Romashkin, P. A. (2015) Aircraft measurements of BrO, IO, glyoxal, NO₂, H₂O, O₂-O₂ and aerosol extinction profiles in the tropics: comparison with aircraft-/ship-based in situ and lidar measurements, *Atmos. Meas. Tech.*, 8(5), 2121–2148, doi:10.5194/amt-8-2121-2015.
- Vrekoussis, M., Wittrock, F., Richter, A., & Burrows, J. P. (2009). Temporal and spatial variability of glyoxal as observed from space. *Atmospheric Chemistry and Physics*, 1, 4485–4504. Retrieved from <http://www.atmos-chem-phys.net/9/4485/2009/acp-9-4485-2009.html>.
- Wittrock, F., Richter, A., Oetjen, H., Burrows, J. P., Kanakidou, M., Myriokefalitakis, S., ... Wagner, T. (2006). Simultaneous global observations of glyoxal and formaldehyde from space. *Geophysical Research Letters*, 33(16), 1–5. <https://doi.org/10.1029/2006GL026310>.